Available online at http://jprm.sms.edu.pk/
Journal of Prime Research in Mathematics, 2026, 135–160

Journal of Prime Research in Mathematics

Impact of Vaccination on COVID-19 using Fractional Operators with Non-local Kernel

Rashmi Sharma[a], Shiv Shankar Sharma[a], Shyamsunder[b,*], Priti Upreti[c]

[a]*Department of Mathematics, Vivekananda Global University, Jaipur, India.*
[b]*Department of Mathematics, SRM University Delhi-NCR, Sonepat-131029, Haryana, India.*
[c]*Department of Mathematics, Motilal Nehru College, University of Delhi, Delhi, India.*

Abstract

This work analyzes a COVID-19 model that uses a seven-dimensional set of ordinary differential equations to account for the population's first and second vaccination doses. We develop a mathematically nonlinear model of COVID-19 dynamics in integer order and modify it by incorporating the Atangana-Baleanu fractional derivative operator. The existence and stability conditions for the model are verified using Banach's fixed-point theory and Picard's successive approximation techniques. We explore how the model's parameters affect the reproduction number. The applicability of the proposed fractional mathematical model is demonstrated through numerical simulations using memory index values of 0.7, 0.75, 0.8, 0.85, 0.9, 0.95, and 1. Maintaining a virus-free population requires reducing transmission rates and increasing recovery rates among unvaccinated individuals. This can be achieved by rigorously adhering to preventive measures and ensuring early, adequate treatment for infected, unvaccinated individuals.

Keywords: Atangana-Baleanu Fractional Derivative, Basic Reproduction Number, Laplace Transform, COVID-19.

2010 Mathematics Subject Classification: 26A33, 34A08, 37N25, 65P99, 92D30

1. Introduction

A rapidly developing area of mathematics known as fractional calculus has a significant impact on topics related to daily life. It is a generalization of classical calculus. It also includes complex numbers in its fractional-order differentiation and integration. In recent years, many scholars have been interested in this field because of its qualities, extension complexity, and wide range of applications in nearly every branch of mathematics. There are various applications for fractional calculus in science and engineering, such as diffuse potential theory, rheology model, fluid flow, electrical transmission lines, probability image processing, electrochemistry, scattering theory, transport theory, statistics, and viscoelasticity theory. It

*Corresponding author
Email addresses: rrashmi.ravat@gmail.com (Rashmi Sharma), shiv.shankar@vgu.ac.in (Shiv Shankar Sharma), skumawatmath@gmail.com (Shyamsunder), priti.69upreti@gmail.com (Priti Upreti)

Received : 14 October 2025*; Accepted:* 21 March 2026*; Published Online:* 03 April 2026

is also used in numerous fields of mathematical analysis, such as differential and integral equations and operational calculus [20, 55, 27, 31].

Mathematical modeling plays a crucial role in representing real-world phenomena and understanding the mechanisms governing disease transmission. Such models help identify key factors affecting the spread of infections, estimate outbreak severity, and support effective control strategies. Although integer-order differential equations are widely used in biological modeling, they often fail to account for memory and hereditary effects present in many biological systems. Fractional differential equations overcome this limitation by incorporating nonlocal properties, allowing the present state of a system to depend on its past behavior, thereby providing a more realistic description of disease dynamics [39, 23, 50].

In an important advancement in fractional calculus, Atangana and Baleanu introduced fractional operators based on the Mittag–Leffler function [4]. Various fractional derivatives, such as the conformable fractional derivative [41], Caputo–Fabrizio, Riemann–Liouville [3], and the Atangana–Baleanu–Caputo (ABC) fractional derivative, have been applied in disease modeling. Among these, the ABC fractional derivative is preferred due to its nonlocal structure and non-singular Mittag–Leffler kernel, which enables an improved representation of memory effects. Compared to the local conformable operator and the exponential or singular kernels of Caputo–Fabrizio and Riemann–Liouville derivatives, the ABC operator offers greater flexibility and physical relevance for modeling complex epidemiological dynamics [46, 5].

The severe acute respiratory syndrome coronavirus 2 (SARS-CoV-2), responsible for COVID-19, first emerged in China in late 2019 and rapidly evolved into a major global health crisis. Due to its high transmissibility, the virus spread swiftly across China and subsequently to the rest of the world, leading to widespread infections and millions of fatalities. Recognizing the severity of the outbreak, the World Health Organization (WHO) declared COVID-19 a global pandemic in February 2020 [26]. Since then, the pandemic has posed unprecedented challenges to public health systems, economies, and social structures worldwide, causing disturbances at nearly every level of society [53].

Mathematical modeling has long played a crucial role in understanding and predicting the spread of infectious diseases. The foundations of epidemiological modeling can be traced back to the pioneering work of Daniel Bernoulli in 1760 [15], followed by the classical compartmental framework introduced by Kermack and McKendrick [22]. Building on these foundational models, a vast body of literature has emerged focusing on COVID-19 transmission dynamics, highlighting the richness and diversity of modeling approaches used to study the disease [8, 2, 51, 25].

Vaccination has been recognized as one of the most effective public health strategies for controlling infectious diseases in modern medicine [40]. Vaccines stimulate the immune system to develop protection against pathogens, thereby reducing disease severity and mortality [16]. Achieving high vaccination coverage is essential for safeguarding healthcare systems and minimizing the burden of infections. Although vaccination is a collective social responsibility, concerns related to vaccine safety and potential side effects remain significant and must be carefully addressed [18].

In response to the COVID-19 crisis, scientists and healthcare professionals worldwide undertook intensive efforts to develop effective vaccines and antiviral treatments. In India, the vaccination campaign commenced on January 16, 2021, with the second dose administered three to four weeks after the first. Despite the high efficacy of available vaccines, it is important to assess their impact considering imperfect transmission-blocking effects [12]. Consequently, several studies have sought to enhance COVID-19 models by incorporating the effects of imperfect vaccination strategies [29, 28]. Moreover, Pearson et al. [37] demonstrated that COVID-19 vaccination programs can be cost-effective or even cost-saving in low- and middle-income countries when vaccines are affordable and highly effective.

Recent advances in fractional calculus have further enriched the mathematical modeling of epidemiological processes. Techniques such as conformable finite element methods [43] and general fractal derivatives [42] have expanded the analytical and computational capabilities of fractional-order models. Within this evolving framework, the Atangana–Baleanu–Caputo fractional operator has gained attention due to its nonsingular Mittag–Leffler kernel, which enables an effective representation of memory and hereditary effects in disease dynamics. As a result, the ABC fractional framework offers a reliable and efficient approach for

capturing the complex transmission mechanisms of COVID-19 [19, 9, 1].

A growing number of studies have employed fractional-order mathematical models to investigate the spread and control of COVID-19 [21, 33, 11]. Related works have explored various aspects of the pandemic, including post-vaccination health outcomes [32], transmission dynamics and treatment strategies in India [44], vaccine development [13], public perception of immunization [14], large-scale vaccination programs [6], and optimal allocation strategies [17]. More recently, compartmental models incorporating vaccination and quarantine have been proposed [56], while Pandey et al. [36] introduced a non-integer-order COVID-19 model using the ABC fractional derivative to describe crowding effects of the virus, establishing existence and uniqueness through fixed-point theory.

The manuscript is organized as follows: Section 2 provides the necessary mathematical preliminaries for the analysis, including essential concepts of fractional calculus and the Atangana-Baleanu-Caputo fractional derivative. In Section 3, the proposed COVID-19 compartmental model is formulated. Section 4 investigates the qualitative characteristics of the model, including the analysis of the existence and uniqueness of the solution, as well as the positivity and boundedness properties that ensure the biological feasibility of the model. Section 5 is dedicated to the development of an iterative scheme for the COVID-19 model, followed by a detailed stability analysis of the proposed iterative approach. In Section 6, the basic reproduction number is derived using the next-generation matrix method. This section also includes a sensitivity analysis to identify the most influential epidemiological parameters and a local stability analysis of the disease-free equilibrium point. Section 7 describes the numerical scheme used to approximate the fractional-order model. Section 8 presents the numerical simulations and provides a comprehensive discussion of the obtained results, highlighting the effects of vaccination and the memory parameter on the disease dynamics. Finally, Section 9 concludes the paper with a summary of the main findings, and a subsection on future scope outlines potential extensions of the current work.

2. Mathematical Preliminaries

The following specific mathematical formulas are used in this section:

Definition 2.1. The Riemann-Liouville (R-L) fractional integral operator ${}_0\mathscr{D}_t^{-\mu}$ [38] is described as:

$$ {}_0\mathscr{D}_t^{-\mu} g(t) = \frac{1}{\Gamma(\mu)} \int_0^t (t-w)^{\mu-1} g(w)\, dw, \qquad t, \Re(\mu) > 0. \tag{2.1} $$

Definition 2.2. The Caputo fractional derivative [45] is defined as:

$$ {}_0^c\mathscr{D}_t^{-\mu} g(t) = \frac{1}{\Gamma(1-\mu)} \int_0^t \frac{g'(s)}{(t-s)^{\mu}} ds, \qquad t \geq 0;\ 0 < \mu \leq 1. \tag{2.2} $$

Definition 2.3. The fractional derivative in the Caputo sense of Atangana-Baleanu [4] is provided by

$$ {}_0^{ABC}\mathscr{D}_t^{-\mu} g(t) = \frac{M(\mu)}{1-\mu} \int_0^t g'(s) E_{\kappa}\left(\frac{-(t-s)^{\mu}\mu}{1-\mu}\right) ds, \quad n-1 < \mu \leq n, \tag{2.3} $$

where $\mu \in \mathbb{R}$, $M(\mu) > 0$ is normalization function satisfying $M(0) = 1 = M(1)$.

The Mittag-Leffler function denoted by $E_{\kappa}(z)$ as defined as:

$$ E_{\kappa}(z) = \sum_{r=0}^{\infty} \frac{z^r}{\Gamma(\kappa r + 1)}, \quad (\kappa > 0). \tag{2.4} $$

The ABC derivative's corresponding fractional integral is provided by

$$ {}_0^{ABC} I_t^{\mu} g(t) = \frac{1}{M(\mu)} \left((1-\mu) g(t) + \frac{\mu}{\Gamma(\mu)} \int_0^t (t-s)^{\mu} g(s) ds \right). \tag{2.5} $$

Definition 2.4. For piecewise continuous functions g(t) of exponential order $\mu > 0$ for variable t, the Laplace transform (LT) [47] is defined as follows:

$$L[g(t);q] = \overline{g}(q) = \int_0^\infty e^{-qt} g(t)dt, \quad t \geq 0, \ \Re(q) > \mu. \tag{2.6}$$

The standard definition of the inverse LT [47] for the function $\overline{g}(q)$ is expressed as:

$$L[\overline{g}(q);t] = g(t) = \frac{1}{2\pi i}\int_{\sigma-\infty}^{\sigma+\infty} e^{qt}\overline{g}(q)dq, \tag{2.7}$$

where σ is the constant real number.

Definition 2.5. The LT of ABC derivative [4] is as follows:

$$L[{}_0^{ABC}\mathscr{D}_t^{-\mu} g(t)](s) = \frac{M(\mu)}{1-\mu}\frac{s^\mu L[g(t)(s)] - s^{\mu-1}g(0)}{s^\mu + \frac{\mu}{1-\mu}}. \tag{2.8}$$

3. COVID-19 Model

Imagine a population with Homogeneous mixing, meaning that every member has an equal chance of coming into contact with every other member. Deterministic compartmental modeling is used to describe the dynamics of disease transmission. At any given time t, the entire population $N(t)$ is further divided into seven epidemiological states based on the health status of the individual which is as follows:
a) Susceptible individuals = $S(t)$,
b) Exposed individuals = $E(t)$,
c) Symptomatic individuals infected without vaccination = $X(t)$,
d) Symptomatic individuals infected after the initial dose of vaccination = $Y(t)$,
e) Symptomatic individuals infected after receiving the second dose of vaccination = $Z(t)$,
f) Recovered individuals = $R(t)$,
g) Dead individuals = $D(t)$.
At any time t, $N(t)$ is described as the total number of humans, is provided by
$N(t) = S(t) + E(t) + X(t) + Y(t) + Z(t) + R(t) + D(t)$.
The non-linear integer order of the mathematical model of COVID-19 is defined by,

$$\begin{aligned}
\frac{dS(t)}{dt} &= \Lambda - (\delta + \lambda)S(t),\\
\frac{dE(t)}{dt} &= \lambda S(t) - (\delta + \upsilon_x + \upsilon_y + \upsilon_z)\, E(t),\\
\frac{dX(t)}{dt} &= \upsilon_x E(t) - (\delta + \omega_x + \phi_x)\, X(t),\\
\frac{dY(t)}{dt} &= \upsilon_y E(t) - (\delta + \omega_y + \phi_y)\, Y(t),\\
\frac{dZ(t)}{dt} &= \upsilon_z E(t) - (\delta + \omega_z + \phi_z)\, Z(t),\\
\frac{dR(t)}{dt} &= \omega_x X(t) + \omega_y Y(t) + \omega_z Z(t) - \delta R(t),\\
\frac{dD(t)}{dt} &= \phi_x X(t) + \phi_y Y(t) + \phi_z Z(t).
\end{aligned} \tag{3.1}$$

The parameter λ represents the infection rate exponent, which determines the rate at which susceptible individuals contract the illness from symptomatic individuals who are unvaccinated, those who have received the first dose of the vaccine, and those who have received the second dose. This is given as: $\lambda = \frac{\varsigma(X+\alpha Y+\beta Z)}{N}$,

and with the initial conditions being non-negative and defined as,
$S(0)=S_0$, $E(0)=E_0$, $X(0)=X_0$, $Y(0)=Y_0$, $Z(0)=Z_0$, $R(0)=R_0$, $D(0)=D_0$.

All of the model's parameters are defined in the manner described below:

ς	is the transmission rate,
Λ	is the birth rate,
α	is the class Y infection's modification factor,
β	is the class Z infection's modification factor,
δ	is the natural death rate,
$\omega_x, \omega_y, \omega_z$	are the recovery rates from classes X, Y, and Z respectively,
$\upsilon_x, \upsilon_y, \upsilon_z$	are the conversion rates from the exposed class E to classes X, Y, and Z, respectively,
ϕ_x, ϕ_y, ϕ_z	are the COVID-19 disease mortality rates for individuals in classes X, Y, and Z respectively.

Moving forward, we utilize a novel framework that employs a fractional derivative with the Mittag–Leffler kernel, as described below, allowing the model to capture non-local temporal memory effects inherent in epidemic and vaccination processes.

$$\begin{aligned}
{}_0^{ABC}\mathscr{D}_t^{-\mu} S(t) &= \Lambda - (\delta + \lambda) S(t), \\
{}_0^{ABC}\mathscr{D}_t^{-\mu} E(t) &= \lambda S(t) - (\delta + \upsilon_x + \upsilon_y + \upsilon_z)\, E(t), \\
{}_0^{ABC}\mathscr{D}_t^{-\mu} X(t) &= \upsilon_x E(t) - (\delta + \omega_x + \phi_x)\, X(t), \\
{}_0^{ABC}\mathscr{D}_t^{-\mu} Y(t) &= \upsilon_y E(t) - (\delta + \omega_y + \phi_y)\, Y(t), \\
{}_0^{ABC}\mathscr{D}_t^{-\mu} Z(t) &= \upsilon_z E(t) - (\delta + \omega_z + \phi_z)\, Z(t), \\
{}_0^{ABC}\mathscr{D}_t^{-\mu} R(t) &= \omega_x X(t) + \omega_y Y(t) + \omega_z Z(t) - \delta R(t), \\
{}_0^{ABC}\mathscr{D}_t^{-\mu} D(t) &= \phi_x X(t) + \phi_y Y(t) + \phi_z Z(t),
\end{aligned} \tag{3.2}$$

where $\mu \in (0, 1]$.

4. Qualitative Characteristics of the Model

This section presents a comprehensive analysis of the proposed model (3.2), emphasizing fundamental properties such as the existence and uniqueness of solutions, along with their positivity and bounded behavior. The discussion highlights the mathematical soundness of the model and explores its relevance and implications within a broader theoretical framework.

4.1. Analysis of Solution Existence and Uniqueness

Let all considered quantities are positive real numbers, represented by $\mathbb{R}_+$ and we assume that $\Delta = \big\{\{S, E, X, Y, Z, R, D\} \in \mathbb{R}_+^7 \ : \ S, E, X, Y, Z, R, D \geq 0,$
$\max\left(|S|, |E|, |X|, |Y|, |Z|, |R|, |D|\right) \leq N\big\}$. Within the region, $\Delta \times (0, T]$, it is established that the fractional-order model (3.2) admits a unique solution.

Theorem 4.1. *Let* $\Upsilon_0 = \big(S(0), E(0), X(0), Y(0), Z(0), R(0), D(0)\big) \in \Delta$ *denote the initial condition of the system. Then, the solution* $\Upsilon = \big(S(t), E(t), X(t), Y(t), Z(t), R(t), D(t)\big)$ *of the fractional-order model* (3.2) *exists uniquely in* Δ *for all* $t \geq 0$.

Proof.

$$\begin{aligned}
\mathfrak{J}_1(\Upsilon) &= \Lambda - (\delta+\lambda)S(t),\\
\mathfrak{J}_2(\Upsilon) &= \lambda S(t) - (\delta+\upsilon_x+\upsilon_y+\upsilon_z)\,E(t),\\
\mathfrak{J}_3(\Upsilon) &= \upsilon_x E(t) - (\delta+\omega_x+\phi_x)\,X(t),\\
\mathfrak{J}_4(\Upsilon) &= \upsilon_y E(t) - (\delta+\omega_y+\phi_y)\,Y(t)\\
\mathfrak{J}_5(\Upsilon) &= \upsilon_z E(t) - (\delta+\omega_z+\phi_z)\,Z(t),\\
\mathfrak{J}_6(\Upsilon) &= \omega_x X(t) + \omega_y Y(t) + \omega_z Z(t) - \delta R(t),\\
\mathfrak{J}_7(\Upsilon) &= \phi_x X(t) + \phi_y Y(t) + \phi_z Z(t),
\end{aligned}$$

for $\Upsilon, \overline{\Upsilon} \in \Delta$, we get

$$\begin{aligned}
&\left\|\mathfrak{J}(\overline{\Upsilon}) - \mathfrak{J}(\Upsilon)\right\| = \left\|\mathfrak{J}_1(\overline{\Upsilon}) - \mathfrak{J}_1(\Upsilon)\right\| + \left\|\mathfrak{J}_2(\overline{\Upsilon}) - \mathfrak{J}_2(\Upsilon)\right\| + \left\|\mathfrak{J}_3(\overline{\Upsilon}) - \mathfrak{J}_3(\Upsilon)\right\|\\
&+ \left\|\mathfrak{J}_4(\overline{\Upsilon}) - \mathfrak{J}_4(\Upsilon)\right\| + \left\|\mathfrak{J}_5(\overline{\Upsilon}) - \mathfrak{J}_5(\Upsilon)\right\| + \left\|\mathfrak{J}_6(\overline{\Upsilon}) - \mathfrak{J}_6(\Upsilon)\right\| + \left\|\mathfrak{J}_7(\overline{\Upsilon}) - \mathfrak{J}_7(\Upsilon)\right\|\\
&\leq (\delta+\lambda)\left\|\overline{S} - S\right\| + (\delta+\upsilon_x+\upsilon_y+\upsilon_z)\left\|\overline{E} - E\right\| + (\delta+\omega_x+\phi_x)\left\|\overline{X} - X\right\|\\
&+ (\delta+\omega_y+\phi_y)\left\|\overline{Y} - Y\right\| + (\delta+\omega_z+\phi_z)\left\|\overline{Z} - Z\right\| + \delta\left\|\overline{R} - R\right\|\\
&+ (\phi_x+\phi_y+\phi_z)\left\|\overline{D} - D\right\| \;\leq \mathcal{M}\left\|\overline{\Upsilon} - \Upsilon\right\|.
\end{aligned}$$

where $\mathcal{M} = max\{(\delta+\lambda), (\delta+\upsilon_x+\upsilon_y+\upsilon_z), (\delta+\omega_x+\phi_x), (\delta+\omega_y+\phi_y), (\delta+\omega_z+\phi_z), (\delta), (\phi_x+\phi_y+\phi_z)\}$. As a consequence, the operator $\mathfrak{J}(\Upsilon)$ satisfies the Lipschitz condition, which guarantees the existence and uniqueness of the solution to the fractional-order model (3.2). □

4.2. Positivity and Boundedness Analysis

Theorem 4.2. *Let the initial conditions of the model belong to the feasible set. Then, the solution of system* (3.2) *preserves positivity for all* $t \geq 0$.

Proof.

$$\begin{aligned}
&{}_0^{ABC}\mathscr{D}_t^{\mu} S(t) = \Lambda - (\delta+\lambda)S(t), \quad 0 < \mu < 1,\\
&{}_0^{ABC}\mathscr{D}_t^{\mu} S(t) \geq -(\delta+\lambda)S(t).
\end{aligned}$$

Taking the Laplace transform on both sides and using the Laplace transform of the Atangana-Baleanu fractional derivative in the Caputo sense, we obtain:

$$\frac{M(\mu)}{1-\mu}\frac{s^{\mu}S(t) - s^{\mu-1}S(0)}{s^{\mu} + \dfrac{\mu}{1-\mu}} \geq -(\delta+\lambda)S(t).$$

Rearranging the above inequality, we get

$$S(t) \geq \frac{s^{\mu-1}}{s^{\mu} + (\delta+\lambda)}\,S(0).$$

Taking inverse Laplace transform, we obtain

$$S(t) \geq E_{\mu,1}(-(\delta+\lambda)t^{\mu})\,S(0).$$

For $\mu \to 1$, the Mittag–Leffler function reduces to the exponential function,

$$E_{1,1}(-(\delta+\lambda)t) = \exp(-(\delta+\lambda)t)\,.$$

Hence, $S(t) \geq \exp(-(\delta+\lambda)t)\,S(0) \geq 0$.

Therefore, $S(t) \geq 0$ for all $t \geq 0$. Similarly,

$$E(t),\ X(t),\ Y(t),\ Z(t),\ R(t),\ D(t) \geq 0.$$

Hence, all state variables of system (3.2) remain non-negative for all $t \geq 0$, ensuring the biological feasibility and well-posedness of the proposed fractional-order COVID-19 model. □

Theorem 4.3. *The solution of the fractional order model* (3.2) *is uniformly bounded in the region* $\Delta^+ = \left\{(S, E, X, Y, Z, R, D) \in \mathbb{R}^7_+ : 0 \leq S + E + X + Y + Z + R + D \leq \frac{\Lambda}{\delta}\right\}$.

Proof. Let $N(t) = S(t) + E(t) + X(t) + Y(t) + Z(t) + R(t) + D(t)$, denote the total population at time t.

Taking the direct sum of all seven equations of the model and using the linearity of the operator, we obtain

$$\begin{aligned} {}^{ABC}_{0}\mathscr{D}_t^{-\mu} N(t) = \Lambda - \delta S(t) - \delta E(t) - (\delta + \omega_x + \phi_x)X(t) - (\delta + \omega_y + \phi_y)Y(t) \\ - (\delta + \omega_z + \phi_z)Z(t) - \delta R(t) + \phi_x X(t) + \phi_y Y(t) + \phi_z Z(t). \end{aligned}$$

Simplifying the above expression, we get

$${}^{ABC}_{0}\mathscr{D}_t^{-\mu} N(t) = \Lambda - \delta\big(S(t) + E(t) + X(t) + Y(t) + Z(t) + R(t)\big) - \omega_x X(t) - \omega_y Y(t) - \omega_z Z(t).$$

Since all state variables are non–negative, it follows that

$${}^{ABC}_{0}\mathscr{D}_t^{-\mu} N(t) \leq \Lambda - \delta N(t).$$

Hence, ${}^{ABC}_{0}\mathscr{D}_t^{-\mu} N(t) + \delta N(t) \leq \Lambda$.

Applying the comparison principle for fractional differential equations (see [24]), we obtain

$$0 \leq N(t) \leq N(0)E_\mu(-\delta t^\mu) + \frac{\Lambda}{\delta}\left[1 - E_{\mu,1}(-\delta t^\mu)\right],$$

where $E_\mu(\cdot)$ and $E_{\mu,1}(\cdot)$ denote the Mittag–Leffler functions.

Taking the limit as $t \to \infty$, we obtain

$$0 \leq N(t) \leq \frac{\Lambda}{\delta}.$$

Therefore, the solution of the fractional order model is uniformly bounded in the region Δ^+, provided the initial conditions lie in Δ^+. This completes the proof. □

5. Iterative Scheme and Stability Analysis of COVID-19 Model

5.1. Iterative Scheme

We derive the ABC fractional model's iterative scheme by following the authors' ideas [44]. In the COVID-19 model (3.2), by applying the Laplace transform to both sides of the fractional differential equations, we obtain

$$\begin{aligned} L[{}^{ABC}_{0}\mathscr{D}_t^{-\mu} S(t)] &= L[\Lambda - (\delta + \lambda)S(t)], \\ L[{}^{ABC}_{0}\mathscr{D}_t^{-\mu} E(t)] &= L[\lambda S(t) - (\delta + \upsilon_x + \upsilon_y + \upsilon_z)\, E(t)], \\ L[{}^{ABC}_{0}\mathscr{D}_t^{-\mu} X(t)] &= L[\upsilon_x E(t) - (\delta + \omega_x + \phi_x)\, X(t)], \end{aligned}$$

$$\begin{aligned} L[{}^{ABC}_{0}\mathscr{D}_t^{-\mu} Y(t)] &= L[\upsilon_y E(t) - (\delta + \omega_y + \phi_y)\, Y(t)], \\ L[{}^{ABC}_{0}\mathscr{D}_t^{-\mu} Z(t)] &= L[\upsilon_z E(t) - (\delta + \omega_z + \phi_z)\, Z(t)], \\ L[{}^{ABC}_{0}\mathscr{D}_t^{-\mu} R(t)] &= L[\omega_x X(t) + \omega_y Y(t) + \omega_z Z(t) - \delta R(t)], \\ L[{}^{ABC}_{0}\mathscr{D}_t^{-\mu} D(t)] &= L[\phi_x X(t) + \phi_y Y(t) + \phi_z Z(t)]. \end{aligned}$$

With the help of equation (2.8), we solve further

$$\frac{M(\mu)}{1-\mu}\frac{x^{\mu}L[S(t)(x)]-x^{\mu-1}S(0)}{x^{\mu}+\frac{\mu}{1-\mu}}=L[\Lambda-(\delta+\lambda)S(t)],$$
$$\frac{M(\mu)}{1-\mu}\frac{x^{\mu}L[E(t)(x)]-x^{\mu-1}E(0)}{x^{\mu}+\frac{\mu}{1-\mu}}=L[\lambda S(t)-(\delta+\upsilon_x+\upsilon_y+\upsilon_z)\,E(t)],$$
$$\frac{M(\mu)}{1-\mu}\frac{x^{\mu}L[X(t)(x)]-x^{\mu-1}X(0)}{x^{\mu}+\frac{\mu}{1-\mu}}=L[\upsilon_x E(t)-(\delta+\omega_x+\phi_x)\,X(t)],$$
$$\frac{M(\mu)}{1-\mu}\frac{x^{\mu}L[Y(t)(x)]-x^{\mu-1}Y(0)}{x^{\mu}+\frac{\mu}{1-\mu}}=L[\upsilon_y E(t)-(\delta+\omega_y+\phi_y)\,Y(t)],$$
$$\frac{M(\mu)}{1-\mu}\frac{x^{\mu}L[Z(t)(x)]-x^{\mu-1}Z(0)}{x^{\mu}+\frac{\mu}{1-\mu}}=L[\upsilon_z E(t)-(\delta+\omega_z+\phi_z)\,Z(t)],$$
$$\frac{M(\mu)}{1-\mu}\frac{x^{\mu}L[R(t)(x)]-x^{\mu-1}R(0)}{x^{\mu}+\frac{\mu}{1-\mu}}=L[\omega_x X(t)+\omega_y Y(t)+\omega_z Z(t)-\delta R(t)],$$
$$\frac{M(\mu)}{1-\mu}\frac{x^{\mu}L[D(t)(x)]-x^{\mu-1}D(0)}{x^{\mu}+\frac{\mu}{1-\mu}}=L[\phi_x X(t)+\phi_y Y(t)+\phi_z Z(t)].$$

By rearranging, we obtain

$$L[S(t);x]=\frac{S(0)}{x}+\frac{x^{\mu}(1-\mu)+\mu}{x^{\mu}M(\mu)}L[\Lambda-(\delta+\lambda)S(t)],$$
$$L[E(t);x]=\frac{E(0)}{x}+\frac{x^{\mu}(1-\mu)+\mu}{x^{\mu}M(\mu)}L[\lambda S(t)-(\delta+\upsilon_x+\upsilon_y+\upsilon_z)\,E(t)],$$

$$L[X(t);x]=\frac{X(0)}{x}+\frac{x^{\mu}(1-\mu)+\mu}{x^{\mu}M(\mu)}L[\upsilon_x E(t)-(\delta+\omega_x+\phi_x)\,X(t)],$$
$$L[Y(t);x]=\frac{Y(0)}{x}+\frac{x^{\mu}(1-\mu)+\mu}{x^{\mu}M(\mu)}L[\upsilon_y E(t)-(\delta+\omega_y+\phi_y)\,Y(t)],$$
$$L[Z(t);x]=\frac{Z(0)}{x}+\frac{x^{\mu}(1-\mu)+\mu}{x^{\mu}M(\mu)}L[\upsilon_z E(t)-(\delta+\omega_z+\phi_z)\,Z(t)],$$
$$L[R(t);x]=\frac{R(0)}{x}+\frac{x^{\mu}(1-\mu)+\mu}{x^{\mu}M(\mu)}L[\omega_x X(t)+\omega_y Y(t)+\omega_z Z(t)-\delta R(t)],$$
$$L[D(t);x]=\frac{D(0)}{x}+\frac{x^{\mu}(1-\mu)+\mu}{x^{\mu}M(\mu)}L[\phi_x X(t)+\phi_y Y(t)+\phi_z Z(t)].$$

By taking the inverse LT, we get

$$
\begin{aligned}
S(t) &= S(0) + L^{-1}\left[\frac{x^{\mu}(1-\mu)+\mu}{x^{\mu}M(\mu)}L[\Lambda-(\delta+\lambda)S(t)]\right],\\
E(t) &= E(0) + L^{-1}\left[\frac{x^{\mu}(1-\mu)+\mu}{x^{\mu}M(\mu)}L[\lambda S(t)-(\delta+\upsilon_x+\upsilon_y+\upsilon_z)\,E(t)]\right],\\
X(t) &= X(0) + L^{-1}\left[\frac{x^{\mu}(1-\mu)+\mu}{x^{\mu}M(\mu)}L[\upsilon_x E(t)-(\delta+\omega_x+\phi_x)\,X(t)]\right],\\
Y(t) &= Y(0) + L^{-1}\left[\frac{x^{\mu}(1-\mu)+\mu}{x^{\mu}M(\mu)}L[\upsilon_y E(t)-(\delta+\omega_y+\phi_y)\,Y(t)]\right],\\
Z(t) &= Z(0) + L^{-1}\left[\frac{x^{\mu}(1-\mu)+\mu}{x^{\mu}M(\mu)}L[\upsilon_z E(t)-(\delta+\omega_z+\phi_z)\,Z(t)]\right],\\
R(t) &= R(0) + L^{-1}\left[\frac{x^{\mu}(1-\mu)+\mu}{x^{\mu}M(\mu)}L[\omega_x X(t)+\omega_y Y(t)+\omega_z Z(t)-\delta R(t)]\right],\\
D(t) &= D(0) + L^{-1}\left[\frac{x^{\mu}(1-\mu)+\mu}{x^{\mu}M(\mu)}L[\phi_x X(t)+\phi_y Y(t)+\phi_z Z(t)]\right].
\end{aligned}
$$

The series solution obtained using the technique is provided by

$$
\begin{aligned}
S &= \sum_{n=0}^{\infty} S_n, \qquad E = \sum_{n=0}^{\infty} E_n, \qquad X = \sum_{n=0}^{\infty} X_n, \qquad Y = \sum_{n=0}^{\infty} Y_n,\\
Z &= \sum_{n=0}^{\infty} Z_n, \qquad R = \sum_{n=0}^{\infty} R_n, \qquad D = \sum_{n=0}^{\infty} D_n.
\end{aligned}
$$

We get the following recursive formulae by using the preliminary conditions,

$$
\begin{aligned}
S_{n+1}(t) &= S_n(0) + L^{-1}\left[\frac{x^{\mu}(1-\mu)+\mu}{x^{\mu}M(\mu)}L[\Lambda-(\delta+\lambda)S_n(t)]\right],\\
E_{n+1}(t) &= E_n(0) + L^{-1}\left[\frac{x^{\mu}(1-\mu)+\mu}{x^{\mu}M(\mu)}L[\lambda S_n(t)-(\delta+\upsilon_x+\upsilon_y+\upsilon_z)\,E_n(t)]\right],\\
X_{n+1}(t) &= X_n(0) + L^{-1}\left[\frac{x^{\mu}(1-\mu)+\mu}{x^{\mu}M(\mu)}L[\upsilon_x E_n(t)-(\delta+\omega_x+\phi_x)\,X_n(t)]\right],\\
Y_{n+1}(t) &= Y_n(0) + L^{-1}\left[\frac{x^{\mu}(1-\mu)+\mu}{x^{\mu}M(\mu)}L[\upsilon_y E_n(t)-(\delta+\omega_y+\phi_y)\,Y_n(t)]\right],\\
Z_{n+1}(t) &= Z_n(0) + L^{-1}\left[\frac{x^{\mu}(1-\mu)+\mu}{x^{\mu}M(\mu)}L[\upsilon_z E_n(t)-(\delta+\omega_z+\phi_z)\,Z_n(t)]\right],\\
R_{n+1}(t) &= R_n(0) + L^{-1}\left[\frac{x^{\mu}(1-\mu)+\mu}{x^{\mu}M(\mu)}L[\omega_x X_n(t)+\omega_y Y_n(t)+\omega_z Z_n(t)-\delta R_n(t)]\right],\\
D_{n+1}(t) &= D_n(0) + L^{-1}\left[\frac{x^{\mu}(1-\mu)+\mu}{x^{\mu}M(\mu)}L[\phi_x X_n(t)+\phi_y Y_n(t)+\phi_z Z_n(t)]\right].
\end{aligned}
\tag{5.1}
$$

5.2. Stability Analysis

Following the concepts described in earlier work [30, 35], we present the stability analysis of the ABC fractional derivative of the COVID-19 model. Let $(B, \|.\|)$ be a Banach space and T is a self-map on B. Also, $K_{n+1} = q(T, K_n)$ represents an exact recurrence formula. A fixed point set of T is denoted by $U(T)$, and there exists at least one element ϱ_n that converges to point $x \in U(T)$. Consider $y_n \in B$ and $j_n = \|y_{n+1} - q(T, y_n)\|$. If $\lim_{n\to\infty} j^n = 0 \Rightarrow \lim_{n\to\infty} y^n = x$. In this case, iteration method $K_{n+1} = q(T, K_n)$ is called T-stable.

Consequently, The sequence y_n is bounded above, which is characteristic of Picard's iteration. It is considered T-stable if all the conditions for the recurrence relation $K_{n+1} = TK_n$ are satisfied.

Proposition 5.1 Let $(B, \|.\|)$ be a Banach space with T as a self-map on B and satisfying

$$\|T_p - T_q\| \leq \tau \|p - T_p\| + \varepsilon \|p - q\|, \qquad \forall\ p, q \in B, \text{ where } 0 \leq \tau, 0 \leq \varepsilon < 1.$$

Then, we conclude T as the Picard T-stable. Moreover, taking into account the connection between (3.1) and (5.1), the following proposition is true:

Proposition 5.2

$$T(S_n(t)) = S_{n+1}(t) = S_n(0) + L^{-1}\left[\frac{x^\mu(1-\mu)+\mu}{x^\mu M(\mu)} L[\Lambda - (\delta+\lambda)S_n(t)]\right],$$
$$T(E_n(t)) = E_{n+1}(t) = E_n(0) + L^{-1}\left[\frac{x^\mu(1-\mu)+\mu}{x^\mu M(\mu)} L[\lambda S_n(t) - (\delta+\upsilon_x+\upsilon_y+\upsilon_z)E_n(t)]\right],$$
$$T(X_n(t)) = X_{n+1}(t) = X_n(0) + L^{-1}\left[\frac{x^\mu(1-\mu)+\mu}{x^\mu M(\mu)} L[\upsilon_x E_n(t) - (\delta+\omega_x+\phi_x)X_n(t)]\right],$$
$$T(Y_n(t)) = Y_{n+1}(t) = Y_n(0) + L^{-1}\left[\frac{x^\mu(1-\mu)+\mu}{x^\mu M(\mu)} L[\upsilon_y E_n(t) - (\delta+\omega_y+\phi_y)Y_n(t)]\right],$$
$$T(Z_n(t)) = Z_{n+1}(t) = Z_n(0) + L^{-1}\left[\frac{x^\mu(1-\mu)+\mu}{x^\mu M(\mu)} L[\upsilon_z E_n(t) - (\delta+\omega_z+\phi_z)Z_n(t)]\right],$$
$$T(R_n(t)) = R_{n+1}(t) = R_n(0) + L^{-1}\left[\frac{x^\mu(1-\mu)+\mu}{x^\mu M(\mu)} L[\omega_x X_n(t) + \omega_y Y_n(t) + \omega_z Z_n(t) - \delta R_n(t)]\right],$$
$$T(D_n(t)) = D_{n+1}(t) = D_n(0) + L^{-1}\left[\frac{x^\mu(1-\mu)+\mu}{x^\mu M(\mu)} L[\phi_x X_n(t) + \phi_y Y_n(t) + \phi_z Z_n(t)]\right],$$

in $L^{-1}(a,b)$, then it is a T-stable if,

$$\begin{aligned}
&(1-(\delta+\lambda)f_1(\mu)) < 1,\\
&(1+\lambda f_2(\mu) - (\delta+\upsilon_x+\upsilon_y+\upsilon_z)f_3(\mu)) < 1,\\
&(1+\upsilon_x f_4(\mu) - (\delta+\omega_x+\phi_x)f_5(\mu)) < 1,\\
&(1+\upsilon_y f_6(\mu) - (\delta+\omega_y+\phi_y)f_7(\mu)) < 1,\\
&(1+\upsilon_z f_8(\mu) - (\delta+\omega_z+\phi_z)f_9(\mu)) < 1,\\
&(1+\omega_x f_{10}(\mu) + \omega_y f_{11}(\mu) + \omega_z f_{12}(\mu) - \delta f_{13}(\mu)) < 1,\\
&(1+\phi_x f_{14}(\mu) + \phi_y f_{15}(\mu) + \phi_z f_{16}(\mu)) < 1.
\end{aligned}$$

Proof:

Since T has a fixed point, the differences for all pairs $(m,n) \in \mathbb{N}\times\mathbb{N}$ are given by:

$$\begin{aligned}
T(S_m(t)) - T(S_n(t)) &= S_m(0) - S_n(0)\\
&\quad + L^{-1}\left[\frac{x^\mu(1-\mu)+\mu}{x^\mu M(\mu)} L[\Lambda - (\delta+\lambda)S_m(t)]\right]\\
&\quad - L^{-1}\left[\frac{x^\mu(1-\mu)+\mu}{x^\mu M(\mu)} L[\Lambda - (\delta+\lambda)S_n(t)]\right],\\
T(E_m(t)) - T(E_n(t)) &= E_m(0) - E_n(0)\\
&\quad + L^{-1}\left[\frac{x^\mu(1-\mu)+\mu}{x^\mu M(\mu)} L[\lambda S_m(t) - (\delta+\upsilon_x+\upsilon_y+\upsilon_z)E_m(t)]\right]\\
&\quad - L^{-1}\left[\frac{x^\mu(1-\mu)+\mu}{x^\mu M(\mu)} L[\lambda S_n(t) - (\delta+\upsilon_x+\upsilon_y+\upsilon_z)E_n(t)]\right],
\end{aligned}$$

$$T\left(X_m(t)\right)-T\left(X_n(t)\right)=X_m(0)-X_n(0)+L^{-1}\left[\frac{x^{\mu}(1-\mu)+\mu}{x^{\mu}M(\mu)}L[\upsilon_x E_m(t)-(\delta+\omega_x+\phi_x)\,X_m(t)]\right]-L^{-1}\left[\frac{x^{\mu}(1-\mu)+\mu}{x^{\mu}M(\mu)}L[\upsilon_x E_n(t)-(\delta+\omega_x+\phi_x)\,X_n(t)]\right],$$

$$T\left(Y_m(t)\right)-T\left(Y_n(t)\right)=Y_m(0)-Y_n(0)+L^{-1}\left[\frac{x^{\mu}(1-\mu)+\mu}{x^{\mu}M(\mu)}L[\upsilon_y E_m(t)-(\delta+\omega_y+\phi_y)\,Y_m(t)]\right]-L^{-1}\left[\frac{x^{\mu}(1-\mu)+\mu}{x^{\mu}M(\mu)}L[\upsilon_y E_n(t)-(\delta+\omega_y+\phi_y)\,Y_n(t)]\right],$$

$$T\left(Z_m(t)\right)-T\left(Z_n(t)\right)=Z_m(0)-Z_n(0)+L^{-1}\left[\frac{x^{\mu}(1-\mu)+\mu}{x^{\mu}M(\mu)}L[\upsilon_z E_m(t)-(\delta+\omega_z+\phi_z)\,Z_m(t)]\right]-L^{-1}\left[\frac{x^{\mu}(1-\mu)+\mu}{x^{\mu}M(\mu)}L[\upsilon_z E_n(t)-(\delta+\omega_z+\phi_z)\,Z_n(t)]\right],$$

$$T\left(R_m(t)\right)-T\left(R_n(t)\right)=R_m(0)-R_n(0)+L^{-1}\left[\frac{x^{\mu}(1-\mu)+\mu}{x^{\mu}M(\mu)}L[\omega_x X_m(t)+\omega_y Y_m(t)+\omega_z Z_m(t)-\delta R_m(t)]\right]-L^{-1}\left[\frac{x^{\mu}(1-\mu)+\mu}{x^{\mu}M(\mu)}L[\omega_x X_n(t)+\omega_y Y_n(t)+\omega_z Z_n(t)-\delta R_n(t)]\right],$$

$$T\left(D_m(t)\right)-T\left(D_n(t)\right)=D_m(0)-D_n(0)+L^{-1}\left[\frac{x^{\mu}(1-\mu)+\mu}{x^{\mu}M(\mu)}L[\phi_x X_m(t)+\phi_y Y_m(t)+\phi_z Z_m(t)]\right]-L^{-1}\left[\frac{x^{\mu}(1-\mu)+\mu}{x^{\mu}M(\mu)}L[\phi_x X_n(t)+\phi_y Y_n(t)+\phi_z Z_n(t)]\right].$$

calculating each side of the equation's norm while maintaining generality

$$\left\|T\left(S_m(t)\right)-T\left(S_n(t)\right)\right\|=\left\|S_m(0)-S_n(0)+L^{-1}\left[\frac{x^{\mu}(1-\mu)+\mu}{x^{\mu}M(\mu)}L[\Lambda-(\delta+\lambda)S_m(t)]\right]-L^{-1}\left[\frac{x^{\mu}(1-\mu)+\mu}{x^{\mu}M(\mu)}L[\Lambda-(\delta+\lambda)S_n(t)]\right]\right\|. \tag{5.2}$$

By using triangular inequality and further simplifying Equation (5.2) the following results are obtained:

$$\left\|T\left(S_m(t)\right)-T\left(S_n(t)\right)\right\|\leq\left\|S_m(0)-S_n(0)\right\|+L^{-1}\left[\frac{x^{\mu}(1-\mu)+\mu}{x^{\mu}M(\mu)}L[\|-(\delta+\lambda)(S_m(t)-S_n(t)\|]\right],$$

or we can say that

$$\left\|T\left(S_m(t)\right)-T\left(S_n(t)\right)\right\|\leq\left(1-(\delta+\lambda)f_1(\mu)\right)\left\|(S_m(t)-S_n(t)\right\|. \tag{5.3}$$

Similarly, we can obtain

$$\begin{aligned}\|T(E_m(t)) - T(E_n(t))\| &\leq (1 + \lambda f_2(\mu) - (\delta + \upsilon_x + \upsilon_y + \upsilon_z) f_3(\mu)) \\ &\times \|E_m(t) - E_n(t)\|, \\ \|T(X_m(t)) - T(X_n(t))\| &\leq (1 + \upsilon_x f_4(\mu) - (\delta + \omega_x + \phi_x) f_5(\mu)) \\ &\times \|X_m(t) - X_n(t)\|,\end{aligned}$$

$$\begin{aligned}\|T(Y_m(t)) - T(Y_n(t))\| &\leq (1 + \upsilon_y f_6(\mu) - (\delta + \omega_y + \phi_y) f_7(\mu)) \\ &\times \|Y_m(t) - Y_n(t)\|, \\ \|T(Z_m(t)) - T(Z_n(t))\| &\leq (1 + \upsilon_z f_8(\mu) - (\delta + \omega_z + \phi_z) f_9(\mu)) \\ &\times \|Z_m(t) - Z_n(t)\|,\end{aligned} \tag{5.4}$$

$$\begin{aligned}\|T(R_m(t)) - T(R_n(t))\| &\leq (1 + \omega_x f_{10}(\mu) + \omega_y f_{11}(\mu) + \omega_z f_{12}(\mu) - \delta f_{13}(\mu)) \\ &\times \|R_m(t) - R_n(t)\|, \\ \|T(D_m(t)) - T(D_n(t))\| &\leq (1 + \phi_x f_{14}(\mu) + \phi_y f_{15}(\mu) + \phi_z f_{16}(\mu)) \\ &\times \|D_m(t) - D_n(t)\|.\end{aligned}$$

Where,

$$\begin{aligned}&(1 - (\delta + \lambda) f_1(\mu)) < 1, \\ &(1 + \lambda f_2(\mu) - (\delta + \upsilon_x + \upsilon_y + \upsilon_z) f_3(\mu)) < 1, \\ &(1 + \upsilon_x f_4(\mu) - (\delta + \omega_x + \phi_x) f_5(\mu)) < 1, \\ &(1 + \upsilon_y f_6(\mu) - (\delta + \omega_y + \phi_y) f_7(\mu)) < 1, \\ &(1 + \upsilon_z f_8(\mu) - (\delta + \omega_z + \phi_z) f_9(\mu)) < 1, \\ &(1 + \omega_x f_{10}(\mu) + \omega_y f_{11}(\mu) + \omega_z f_{12}(\mu) - \delta f_{13}(\mu)) < 1, \\ &(1 + \phi_x f_{14}(\mu) + \phi_y f_{15}(\mu) + \phi_z f_{16}(\mu)) < 1.\end{aligned}$$

As a result, there is a fixed point on the self-mapping T. We demonstrate that T satisfies every requirement in Proposition 5.1. Since (5.3) and (5.4) are assumed to be true, we utilize $\varepsilon = (0, 0, 0, 0, 0, 0, 0)$ and

$$\tau = \begin{cases} (1 - (\delta + \lambda) f_1(\mu)) < 1, \\ (1 + \lambda f_2(\mu) - (\delta + \upsilon_x + \upsilon_y + \upsilon_z) f_3(\mu)) < 1, \\ (1 + \upsilon_x f_4(\mu) - (\delta + \omega_x + \phi_x) f_5(\mu)) < 1, \\ (1 + \upsilon_y f_6(\mu) - (\delta + \omega_y + \phi_y) f_7(\mu)) < 1, \\ (1 + \upsilon_z f_8(\mu) - (\delta + \omega_z + \phi_z) f_9(\mu)) < 1, \\ (1 + \omega_x f_{10}(\mu) + \omega_y f_{11}(\mu) + \omega_z f_{12}(\mu) - \delta f_{13}(\mu)) < 1, \\ (1 + \phi_x f_{14}(\mu) + \phi_y f_{15}(\mu) + \phi_z f_{16}(\mu)) < 1. \end{cases}$$

Therefore, the self-map T satisfies every requirement in Proposition 5.2. As a result, T is Picard T-stable.

6. Basic Reproduction Number and Sensitivity Analysis

6.1. Basic Reproduction Number

Finding the model's disease-free equilibrium is essential to determining the fundamental reproduction number connected to model (3.2). We refer to the situation where the population has no infections as a disease-free equilibrium. Therefore, model (3.2)'s infectious compartments are all set to zero. It means $E = X = Y = Z = 0$. Furthermore, in model (3.2), set the fractional derivatives of the non-infectious

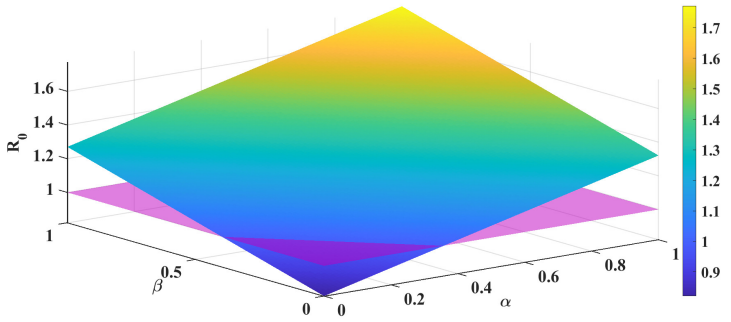

Figure 1: Influence of parameters α and β on the dynamics of the reproductive number.

compartments to zero. That is, ${}^{\text{ABC}}\mathscr{D}_t^{\mu} S(t) = {}^{\text{ABC}}\mathscr{D}_t^{\mu} D(t) = 0$. Hence, $\beth_0$, represents the disease-free equilibrium point, which is given by

$$\beth_0 = \left(S^0,\ E^0,\ X^0,\ Y^0,\ Z^0,\ R^0,\ D^0\right) = \left(\frac{\Lambda}{\delta},\ 0,\ 0,\ 0,\ 0,\ 0,\ 0\right).$$

We now calculate the basic reproduction number for model (3.2) using the next-generation matrix technique, as detailed in [54]. Taking this method into consideration, the matrix $\mathcal{F}$ of the newly evaluated infection terms at $\beth_0$ is provided by

$$\mathcal{F} = \begin{pmatrix} 0 & \varsigma & \alpha\varsigma & \beta\varsigma & 0 \\ 0 & 0 & 0 & 0 & 0 \\ 0 & 0 & 0 & 0 & 0 \\ 0 & 0 & 0 & 0 & 0 \\ 0 & 0 & 0 & 0 & 0 \end{pmatrix},$$

and the matrix $\mathcal{V}$ containing the transition terms at the specified point $\beth_0$ is acquired as

$$\mathcal{V} = \begin{pmatrix} b_1 & 0 & 0 & 0 & 0 \\ -\upsilon_x & b_2 & 0 & 0 & 0 \\ -\upsilon_y & 0 & b_3 & 0 & 0 \\ -\upsilon_z & 0 & 0 & b_4 & 0 \\ 0 & -\omega_x & -\omega_y & -\omega_z & \delta \end{pmatrix},$$

where $b_1 = (\delta + \upsilon_x + \upsilon_y + \upsilon_z)$, $b_2 = (\delta + \omega_x + \phi_x)$, $b_3 = (\delta + \omega_y + \phi_y)$, $b_4 = (\delta + \omega_z + \phi_z)$. Therefore, the required effective reproduction number is the greatest eigenvalue of the next generation matrix $\mathcal{F}\mathcal{V}^{-1}$ is given by

$$\mathcal{R}_0 = \frac{\varsigma\upsilon_x}{b_1 b_2} + \frac{\varsigma\,\alpha\upsilon_y}{b_1 b_3} + \frac{\varsigma\,\beta\upsilon_z}{b_1 b_4}. \tag{6.1}$$

Equation (6.1) encompasses three effective reproduction numbers. The first parameter is $\mathcal{R}_{0X} = \frac{\varsigma\upsilon_x}{b_1 b_2}$, representing the number of new COVID-19 cases arising from the unvaccinated class of infected people (X). The second parameter is $\mathcal{R}_{0Y} = \frac{\varsigma\,\alpha\upsilon_x}{b_1 b_3}$, denoting the number of cases arising from the first dose vaccination class of infected people (Y). The third parameter is $\mathcal{R}_{0Z} = \frac{\varsigma\,\beta\upsilon_z}{b_1 b_4}$, which indicates the number of COVID-19 cases produced from the second dose (fully vaccinated) class of infected individuals (Z). Consequently, the formulation for $\mathcal{R}_0$ in Equation (6.1) can be expressed as

$$\mathcal{R}_0 = \mathcal{R}_{0X} + \mathcal{R}_{0Y} + \mathcal{R}_{0Z}.$$

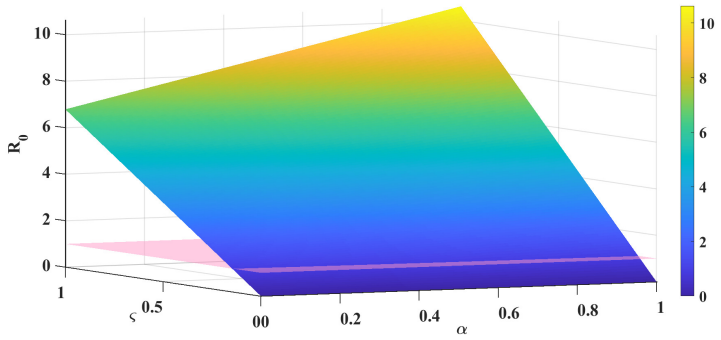

Figure 2: Influence of parameters α and ς on the dynamics of the reproductive number.

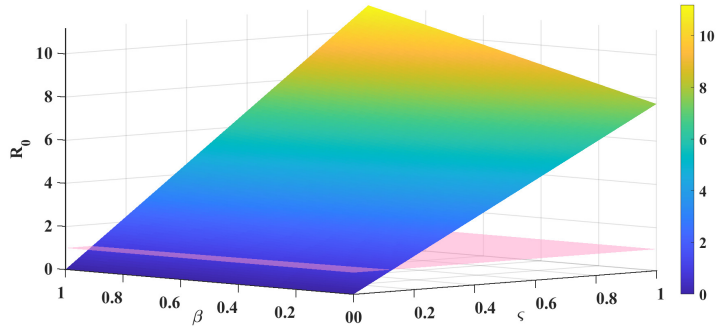

Figure 3: Influence of parameters ς and β on the dynamics of the reproductive number.

6.2. Sensitivity Analysis

In this section, we examine the influence of all parameters involved in the basic reproduction number $\mathcal{R}_0$, as defined in equation (6.1), to assess their roles in disease transmission. The objective is to identify effective intervention measures that can reduce and control the spread of COVID-19 within a population. To achieve this, we adopt the methodological framework proposed in earlier studies [7, 49] and compute the sensitivity indices of $\mathcal{R}_0$ with respect to each model parameter using the following analytical formulation.

$$S_{\varrho}^{\mathcal{R}_0} = \frac{\varrho}{\mathcal{R}_0} \times \frac{\partial \mathcal{R}_0}{\partial \varrho}. \tag{6.2}$$

Here, ϱ denotes any parameter appearing in the expression of $\mathcal{R}_0$ Using relation (6.2), we derive the analytical sensitivity indices of the basic reproduction number with respect to the parameters of model (3.2), which are presented below.

$$\begin{aligned}
S_{\varsigma}^{\mathcal{R}_0} &= \frac{\varsigma}{\mathcal{R}_0}\left[\frac{\upsilon_x}{b_1 b_2} + \frac{\alpha\,\upsilon_y}{b_1 b_3} + \frac{\beta\,\upsilon_z}{b_1 b_4}\right], \\
S_{\alpha}^{\mathcal{R}_0} &= \frac{\alpha}{\mathcal{R}_0}\left[\frac{\varsigma\,\upsilon_y}{b_1 b_3}\right], \\
S_{\beta}^{\mathcal{R}_0} &= \frac{\beta}{\mathcal{R}_0}\left[\frac{\varsigma\,\upsilon_z}{b_1 b_4}\right], \\
S_{\delta}^{\mathcal{R}_0} &= \frac{\delta}{\mathcal{R}_0}\left[-\frac{\varsigma\,\upsilon_x}{b_1^2 b_2} - \frac{\varsigma\,\upsilon_x}{b_1 b_2^2} - \frac{\varsigma\,\alpha\,\upsilon_y}{b_1^2 b_3} - \frac{\varsigma\,\alpha\,\upsilon_y}{b_1 b_3^2} - \frac{\varsigma\,\beta\,\upsilon_z}{b_1^2 b_4} - \frac{\varsigma\,\beta\,\upsilon_z}{b_1 b_4^2}\right],
\end{aligned}$$

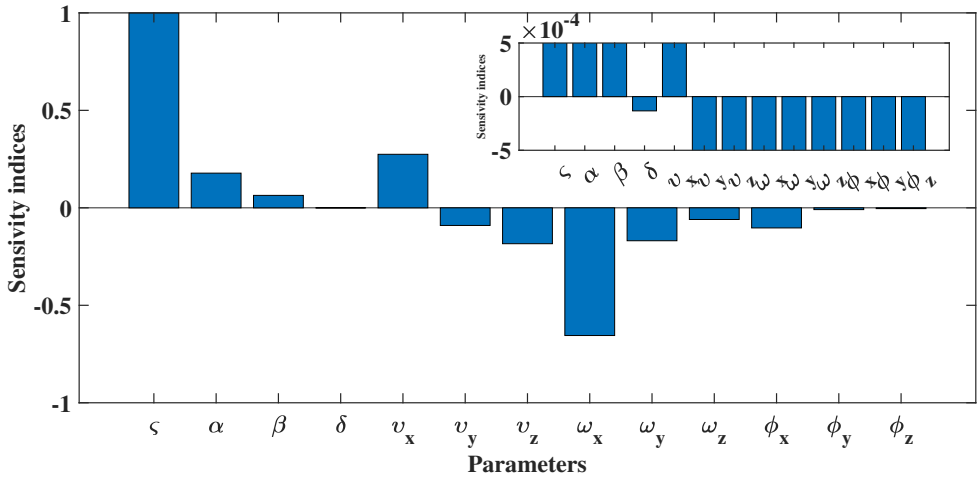

Figure 4: Normalized sensitivity indices of the basic reproduction number with respect to key parameters of the COVID-19 transmission model.

$$
\begin{aligned}
S^{\mathcal{R}_0}_{\upsilon_x} &= \frac{\upsilon_x}{\mathcal{R}_0}\left[\frac{\varsigma}{b_1 b_2} - \frac{\varsigma\,\upsilon_x}{b_1^2 b_2} - \frac{\varsigma\,\alpha\,\upsilon_y}{b_1^2 b_3} - \frac{\varsigma\,\beta\,\upsilon_z}{b_1^2 b_4}\right],\\
S^{\mathcal{R}_0}_{\upsilon_y} &= \frac{\upsilon_y}{\mathcal{R}_0}\left[-\frac{\varsigma\,\upsilon_x}{b_1^2 b_2} + \frac{\varsigma\,\alpha}{b_1 b_3} - \frac{\varsigma\,\alpha\,\upsilon_y}{b_1^2 b_3} - \frac{\varsigma\,\beta\,\upsilon_z}{b_1^2 b_4}\right],\\
S^{\mathcal{R}_0}_{\upsilon_z} &= \frac{\upsilon_z}{\mathcal{R}_0}\left[-\frac{\varsigma\,\upsilon_x}{b_1^2 b_2} - \frac{\varsigma\,\alpha\,\upsilon_y}{b_1^2 b_3} + \frac{\varsigma\,\beta}{b_1 b_4} - \frac{\varsigma\,\beta\,\upsilon_z}{b_1^2 b_4}\right],
\end{aligned}
$$

$$
\begin{aligned}
S^{\mathcal{R}_0}_{\omega_x} &= \frac{\omega_x}{\mathcal{R}_0}\left[-\frac{\varsigma\,\upsilon_x}{b_1 b_2^2}\right],\\
S^{\mathcal{R}_0}_{\omega_y} &= \frac{\omega_y}{\mathcal{R}_0}\left[-\frac{\varsigma\,\alpha\,\upsilon_y}{b_1 b_3^2}\right],\\
S^{\mathcal{R}_0}_{\omega_z} &= \frac{\omega_z}{\mathcal{R}_0}\left[-\frac{\varsigma\,\beta\,\upsilon_z}{b_1 b_4^2}\right],\\
S^{\mathcal{R}_0}_{\phi_x} &= \frac{\phi_x}{\mathcal{R}_0}\left[-\frac{\varsigma\,\upsilon_x}{b_1 b_2^2}\right],\\
S^{\mathcal{R}_0}_{\phi_y} &= \frac{\phi_y}{\mathcal{R}_0}\left[-\frac{\varsigma\,\alpha\,\upsilon_y}{b_1 b_3^2}\right],\\
S^{\mathcal{R}_0}_{\phi_z} &= \frac{\phi_z}{\mathcal{R}_0}\left[-\frac{\varsigma\,\beta\,\upsilon_z}{b_1 b_4^2}\right].
\end{aligned}
$$

Consequently, the numerical sensitivity indices of model (3.2), with $\mathcal{R}_0$ serving as the response function, are computed by substituting the baseline parameter values listed in Table (1) into the derived analytical expressions.

The Figure 4 illustrates the normalized sensitivity indices of the basic reproduction number ($\mathcal{R}_0$) corresponding to various epidemiological parameters of the COVID-19 model. Positive sensitivity indices indicate parameters that enhance disease transmission, while negative indices represent parameters that reduce ($\mathcal{R}_0$). The results show that the transmission intensity (ς) and progression-related parameters (υ_x) have the strongest positive influence on ($\mathcal{R}_0$), whereas recovery and control-related parameters ($\omega_x, \omega_y, \omega_z$) and ($\phi_x, \phi_y, \phi_z$) significantly suppress disease spread. These findings underscore the crucial role of intervention and treatment strategies in mitigating COVID-19 transmission.

6.3. Local Stability Analysis

To study the local stability of the proposed model, we restrict our attention to the alive population, since the death compartment does not contribute to the transmission dynamics and evolves independently of the infection process. Accordingly, the reduced system is analyzed around the disease-free equilibrium [48].

Theorem 6.1. *For the fractional-order model* (3.2) *with* $0 < \mu \leq 1$*, the disease-free equilibrium point* $\beth_0 = \left(\frac{\Lambda}{\delta}, 0, 0, 0, 0, 0, 0\right)$ *is locally asymptotically stable in the feasible region* Δ *if* $\mathcal{R}_0 < 1$*, and unstable if* $\mathcal{R}_0 > 1$*.*

Proof. Consider the fractional-order system (3.2) governed by the Atangana–Baleanu–Caputo fractional derivative. The Jacobian matrix of the system evaluated at the disease-free equilibrium $\beth_0$ is given by

$$\mathfrak{J}(\beth_0) = \begin{pmatrix} -\delta & 0 & -\varsigma\frac{\Lambda}{\delta N} & -\alpha\varsigma\frac{\Lambda}{\delta N} & -\beta\varsigma\frac{\Lambda}{\delta N} & 0 \\ 0 & -b_1 & \varsigma\frac{\Lambda}{\delta N} & \alpha\varsigma\frac{\Lambda}{\delta N} & \beta\varsigma\frac{\Lambda}{\delta N} & 0 \\ 0 & \upsilon_x & -b_2 & 0 & 0 & 0 \\ 0 & \upsilon_y & 0 & -b_3 & 0 & 0 \\ 0 & \upsilon_z & 0 & 0 & -b_4 & 0 \\ 0 & 0 & \omega_x & \omega_y & \omega_z & -\delta \end{pmatrix},$$

where

$$b_1 = \delta + \upsilon_x + \upsilon_y + \upsilon_z, \quad b_2 = \delta + \omega_x + \phi_x, \quad b_3 = \delta + \omega_y + \phi_y, \quad b_4 = \delta + \omega_z + \phi_z.$$

The eigenvalues of the Jacobian matrix are given by

$$\lambda_1 = \lambda_2 = -\delta, \quad \lambda_3 = -b_2, \quad \lambda_4 = -b_3, \quad \lambda_5 = -b_4,$$

and the remaining eigenvalue satisfies

$$\lambda + b_1 - \varsigma\left(\frac{\upsilon_x}{b_2} + \frac{\alpha\upsilon_y}{b_3} + \frac{\beta\upsilon_z}{b_4}\right) = 0.$$

Hence, $\lambda_6 = -b_1\left(1 - \mathcal{R}_0\right)$, where the basic reproduction number is defined as $\mathcal{R}_0 = \frac{\varsigma\upsilon_x}{b_1 b_2} + \frac{\varsigma\alpha\upsilon_y}{b_1 b_3} + \frac{\varsigma\beta\upsilon_z}{b_1 b_4}$.

Since $b_i > 0$ for $i = 1, 2, 3, 4$, all eigenvalues have negative real parts if and only if $\mathcal{R}_0 < 1$. Therefore, the disease-free equilibrium $\beth_0$ is locally asymptotically stable when $\mathcal{R}_0 < 1$ and unstable when $\mathcal{R}_0 > 1$. □

7. Numerical Scheme

This section presents the model simulations after first deriving the numerical solution of the suggested fractional order model (3.2) with the non-local and non-singular kernel. For this reason, we employ the numerical method recently suggested in [52, 10] to approximate the fractional integral AB operator. This recently established numerical technique is obtained by combining the two-step Lagrange polynomial with the fundamental theorem of fractional calculus.

First, we rewrite the model (3.2) in the following simple form by using fixed point theory:

$${}^{\mathrm{ABC}}_{0}\mathscr{D}^{\mu}_{t}\,\vartheta(t) = \mathscr{F}(t, \vartheta(t)), \;\; \vartheta(0) = \vartheta_0. \tag{7.1}$$

Using the fundamental theorem, the following fractional integral equation can represent the system (7.1).

$$\vartheta(t) - \vartheta(0) = \frac{1-\mu}{ABC(\mu)}\mathscr{F}(t, \vartheta(t)) + \frac{\mu}{ABC(\mu) \times \Gamma(\mu)}\int_0^t \mathscr{F}(\varepsilon, \vartheta(\varepsilon))(t-\varepsilon)^{\mu-1}d\varepsilon.$$

At $t = t_{n+1}, n = 0, 1, 2, \ldots$, we have,

$$\vartheta(t_{n+1}) - \vartheta(0) = \frac{1-\mu}{ABC(\mu)}\mathscr{F}(t_n, \vartheta(t_n)) + \frac{\mu}{ABC(\mu) \times \Gamma(\mu)} \int_0^{t_{n+1}} \mathscr{F}(\varepsilon, \vartheta(\varepsilon))(t_{n+1} - \varepsilon)^{\mu-1} d\varepsilon.$$

Which can be written as

$$\vartheta(t_{n+1}) - \vartheta(0) = \frac{1-\mu}{ABC(\mu)}\mathscr{F}(t_n, \vartheta(t_n)) + \frac{\mu}{ABC(\mu) \times \Gamma(\mu)} \sum_{r=0}^{n} \int_{t_r}^{t_{r+1}} \mathscr{F}(\varepsilon, \vartheta(\varepsilon))(t_{n+1} - \varepsilon)^{\mu-1} d\varepsilon. \tag{7.2}$$

The function $\mathscr{F}(\varepsilon, \vartheta(\varepsilon))$ can be approximated over $[t_r, t_{r+1}]$, using the interpolation polynomial

$$\mathscr{F}(\varepsilon, \vartheta(\varepsilon)) \cong \frac{\mathscr{F}(t_r, \vartheta(t_r))}{h}(t - t_{r-1}) - \frac{\mathscr{F}(t_{r-1}, \vartheta(t_{r-1}))}{h}(t - t_r).$$

Putting in Equation (7.2), we get

$$\vartheta(t_{n+1}) = \vartheta(0) + \frac{1-\mu}{ABC(\mu)}\mathscr{F}(t_n, \vartheta(t_n)) + \frac{\mu}{ABC(\mu) \times \Gamma(\mu)} \sum_{r=0}^{n} \Big(\frac{\mathscr{F}(t_r, \vartheta(t_r))}{h} \int_{t_r}^{t_{r+1}} (t - t_{r-1})(t_{n+1} - t)^{\mu-1} dt - \frac{\mathscr{F}(t_{r-1}, \vartheta(t_{r-1}))}{h} \int_{t_r}^{t_{r+1}} (t - t_r)(t_{n+1} - t)^{\mu-1} dt \Big).$$

Calculating these integrals, finally, we get an approximate solution as:

$$\vartheta(t_{n+1}) = \vartheta(t_0) + \frac{1-\mu}{ABC(\mu)}\mathscr{F}(t_n, \vartheta(t_n)) + \frac{\mu}{ABC(\mu)} \sum_{r=0}^{n} \Bigg(\frac{h^\mu \mathscr{F}(t_r, \vartheta(t_r))}{\Gamma(\mu+2)}((n+1-r)^\mu(n-r+2+\mu) - (n-r)^\mu(n-r+2+2\mu)) - \frac{h^\mu \mathscr{F}(t_{r-1}, \vartheta(t_{r-1}))}{\Gamma(\mu+2)}((n+1-r)^{\mu+1} - (n-r)^\mu(n-r+1+\mu)) \Bigg).$$

Now we obtained the following recursive formulae for the model equations:

$$S(t_{n+1}) = S(t_0) + \frac{1-\mu}{ABC(\mu)}\mathscr{F}_1(t_n, \vartheta(t_n)) + \frac{\mu}{ABC(\mu)} \sum_{r=0}^{n} \Bigg(\frac{h^\mu \mathscr{F}_1(t_r, \vartheta(t_r))}{\Gamma(\mu+2)}((n+1-r)^\mu(n-r+2+\mu) - (n-r)^\mu(n-r+2+2\mu)) - \frac{h^\mu \mathscr{F}_1(t_{r-1}, \vartheta(t_{r-1}))}{\Gamma(\mu+2)}((n+1-r)^{\mu+1} - (n-r)^\mu(n-r+1+\mu)) \Bigg).$$

$$E(t_{n+1}) = E(t_0) + \frac{1-\mu}{ABC(\mu)}\mathscr{F}_2(t_n, \vartheta(t_n)) + \frac{\mu}{ABC(\mu)} \sum_{r=0}^{n} \Bigg(\frac{h^\mu \mathscr{F}_2(t_r, \vartheta(t_r))}{\Gamma(\mu+2)}((n+1-r)^\mu(n-r+2+\mu) - (n-r)^\mu(n-r+2+2\mu)) \frac{h^\mu \mathscr{F}_2(t_{r-1}, \vartheta(t_{r-1}))}{\Gamma(\mu+2)}((n+1-r)^{\mu+1} - (n-r)^\mu(n-r+1+\mu)) \Bigg).$$

$$X(t_{n+1}) = X(t_0) + \frac{1-\mu}{ABC(\mu)}\mathscr{F}_3(t_n, \vartheta(t_n)) + \frac{\mu}{ABC(\mu)} \sum_{r=0}^{n}\left(\frac{h^\mu \mathscr{F}_3(t_r, \vartheta(t_r))}{\Gamma(\mu+2)}((n+1-r)^\mu(n-r+2+\mu) - (n-r)^\mu(n-r+2+2\mu)) - \frac{h^\mu \mathscr{F}_3(t_{r-1}, \vartheta(t_{r-1}))}{\Gamma(\mu+2)}((n+1-r)^{\mu+1} - (n-r)^\mu(n-r+1+\mu))\right).$$

$$Y(t_{n+1}) = Y(t_0) + \frac{1-\mu}{ABC(\mu)}\mathscr{F}_4(t_n, \vartheta(t_n)) + \frac{\mu}{ABC(\mu)} \sum_{r=0}^{n}\left(\frac{h^\mu \mathscr{F}_4(t_r, \vartheta(t_r))}{\Gamma(\mu+2)}((n+1-r)^\mu(n-r+2+\mu) - (n-r)^\mu(n-r+2+2\mu)) - \frac{h^\mu \mathscr{F}_4(t_{r-1}, \vartheta(t_{r-1}))}{\Gamma(\mu+2)}((n+1-r)^{\mu+1} - (n-r)^\mu(n-r+1+\mu))\right).$$

$$Z(t_{n+1}) = Z(t_0) + \frac{1-\mu}{ABC(\mu)}\mathscr{F}_5(t_n, \vartheta(t_n)) + \frac{\mu}{ABC(\mu)} \sum_{r=0}^{n}\left(\frac{h^\mu \mathscr{F}_5(t_r, \vartheta(t_r))}{\Gamma(\mu+2)}((n+1-r)^\mu(n-r+2+\mu) - (n-r)^\mu(n-r+2+2\mu)) - \frac{h^\mu \mathscr{F}_5(t_{r-1}, \vartheta(t_{r-1}))}{\Gamma(\mu+2)}((n+1-r)^{\mu+1} - (n-r)^\mu(n-r+1+\mu))\right).$$

$$R(t_{n+1}) = R(t_0) + \frac{1-\mu}{ABC(\mu)}\mathscr{F}_6(t_n, \vartheta(t_n)) + \frac{\mu}{ABC(\mu)} \sum_{r=0}^{n}\left(\frac{h^\mu \mathscr{F}_6(t_r, \vartheta(t_r))}{\Gamma(\mu+2)}((n+1-r)^\mu(n-r+2+\mu) - (n-r)^\mu(n-r+2+2\mu)) - \frac{h^\mu \mathscr{F}_6(t_{r-1}, \vartheta(t_{r-1}))}{\Gamma(\mu+2)}((n+1-r)^{\mu+1} - (n-r)^\mu(n-r+1+\mu))\right).$$

$$D(t_{n+1}) = D(t_0) + \frac{1-\mu}{ABC(\mu)}\mathscr{F}_7(t_n, \vartheta(t_n)) + \frac{\mu}{ABC(\mu)} \sum_{r=0}^{n}\left(\frac{h^\mu \mathscr{F}_7(t_r, \vartheta(t_r))}{\Gamma(\mu+2)}((n+1-r)^\mu(n-r+2+\mu) - (n-r)^\mu(n-r+2+2\mu)) - \frac{h^\mu \mathscr{F}_7(t_{r-1}, \vartheta(t_{r-1}))}{\Gamma(\mu+2)}((n+1-r)^{\mu+1} - (n-r)^\mu(n-r+1+\mu))\right).$$

8. Results and Discussion

Table 1 presents the estimated model parameters obtained during calibration. In this study, parameter values are adopted from established COVID-19 transmission and vaccination-related literature and are selected within biologically realistic ranges [34]. Since the primary emphasis of the present work is on the qualitative dynamics of the model and the influence of fractional-order memory effects, a detailed parameter estimation and data-fitting procedure is not pursued. A comprehensive data-driven calibration, along with uncertainty and sensitivity analyses, may be considered as a potential extension of this model in future

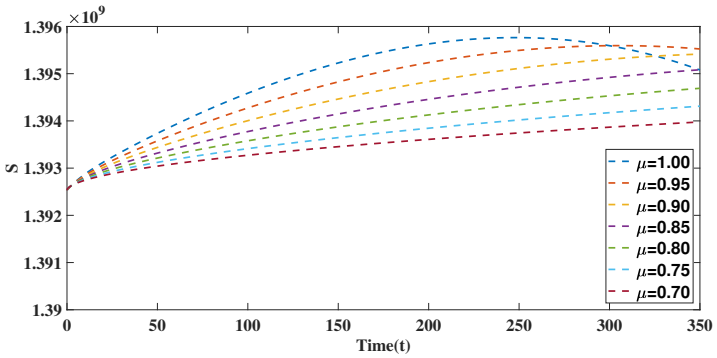

Figure 5: Susceptible people with fractional order μ.

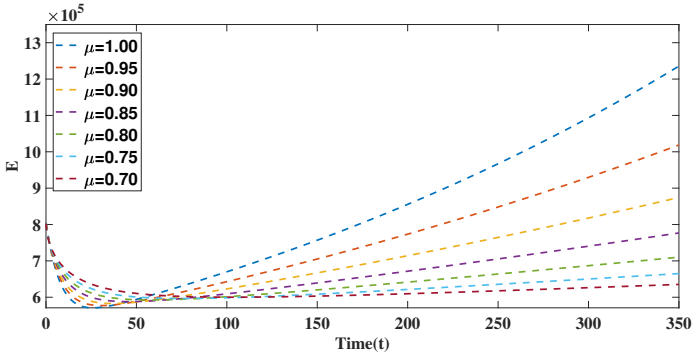

Figure 6: Exposed people with fractional order μ.

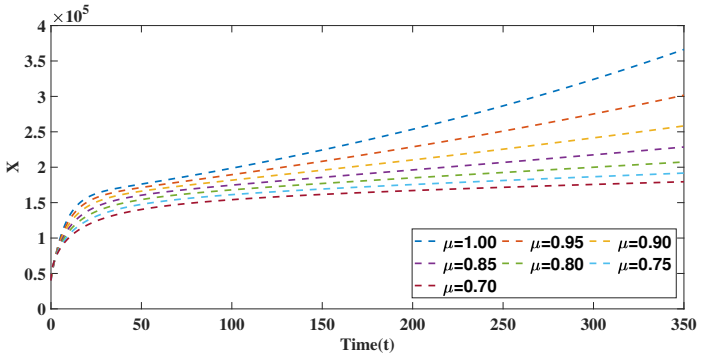

Figure 7: Without vaccinated people with fractional order μ.

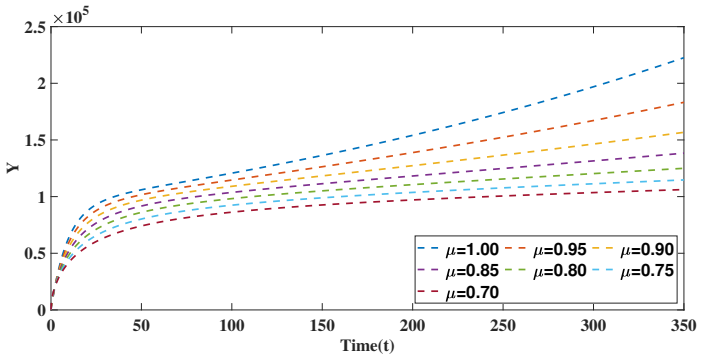

Figure 8: One dose vaccinated people with fractional order μ.

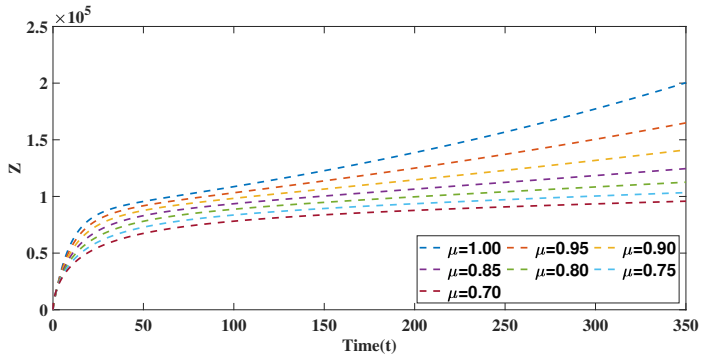

Figure 9: Double dose vaccinated people with fractional order μ.

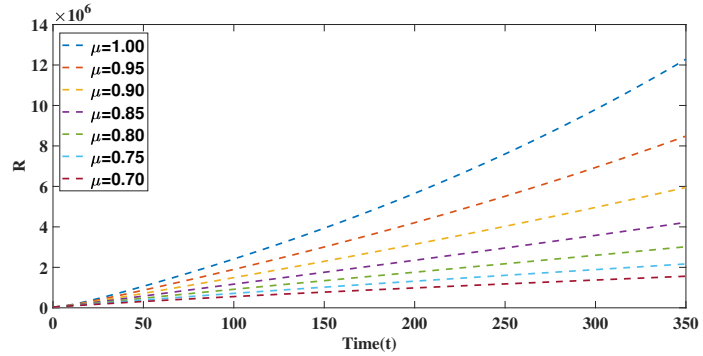

Figure 10: Recovered people with fractional order μ.

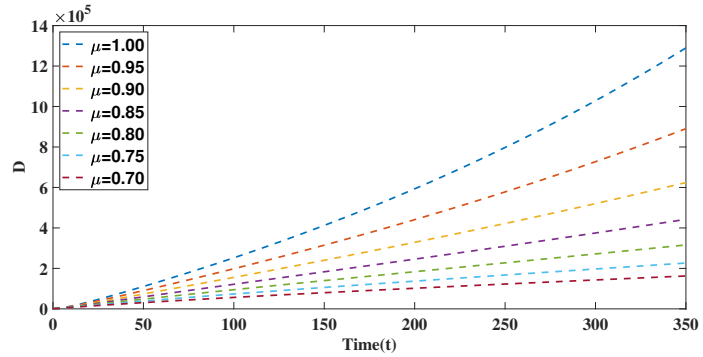

Figure 11: Dead people with fractional order μ.

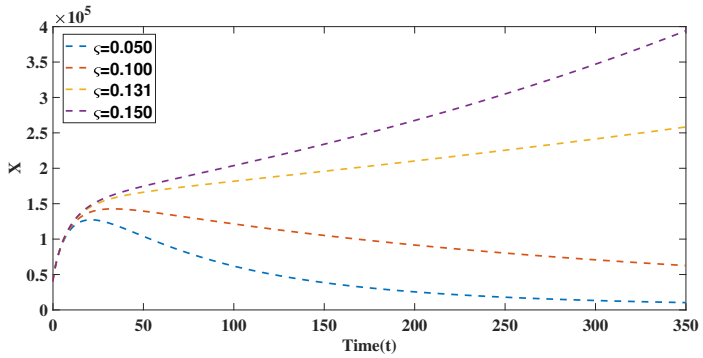

Figure 12: The impact of transmission rates on the unvaccinated population.

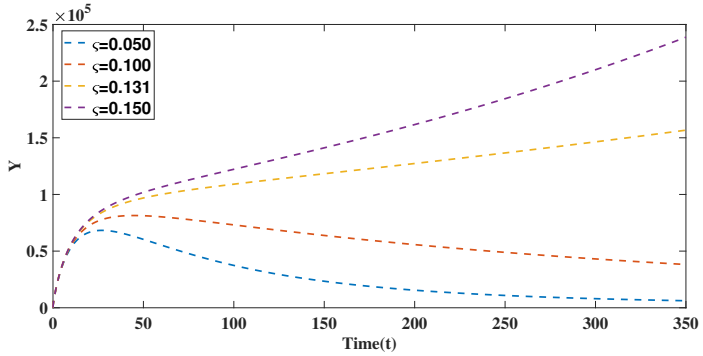

Figure 13: The impact of transmission rates on a population that has received a single vaccination dose.

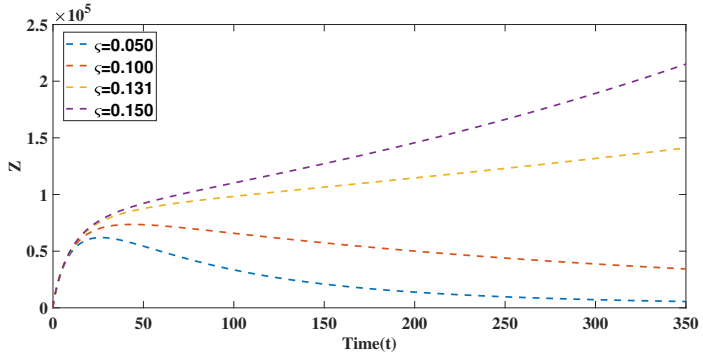

Figure 14: The impact of transmission rates on a population that has received a double vaccination dose.

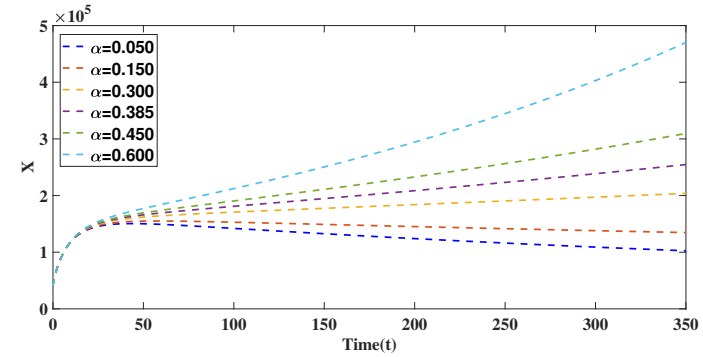

Figure 15: The effect of modification rate α on the unvaccinated population.

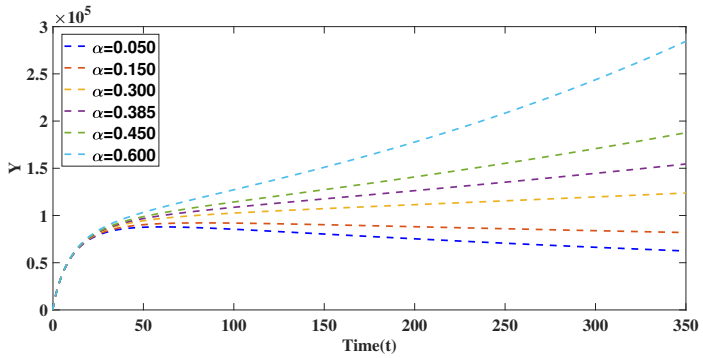

Figure 16: The effect of modification rate α on a single-dose vaccinated population.

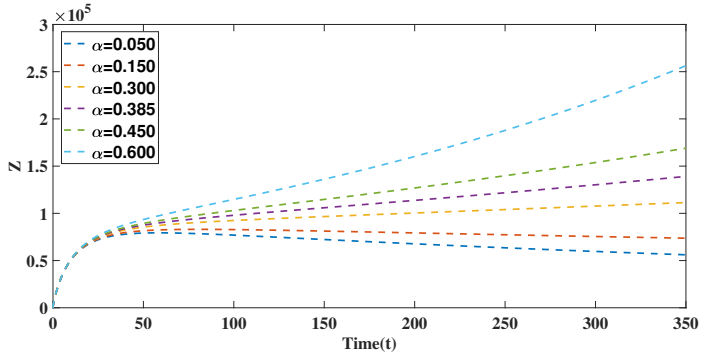

Figure 17: The effect of modification rate α on a double dose vaccinated population.

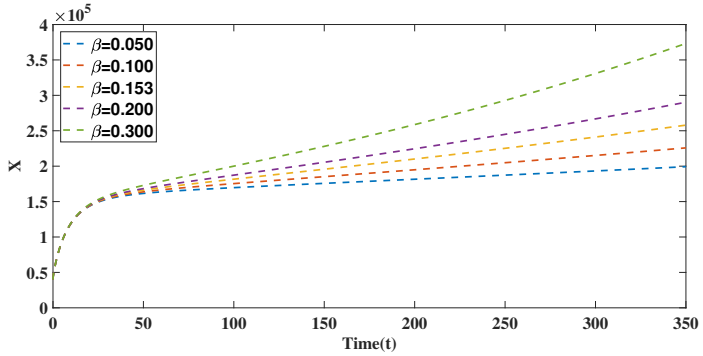

Figure 18: The effect of modification rate β on the unvaccinated population.

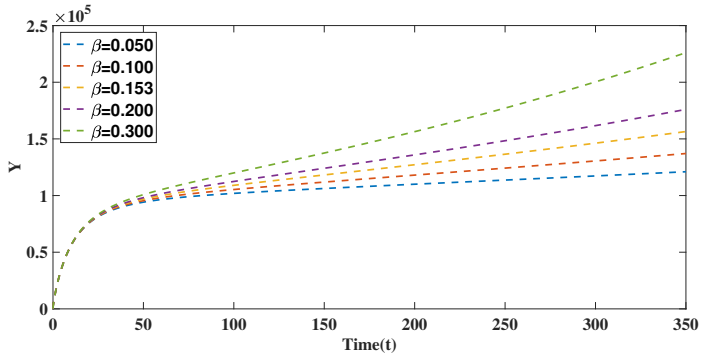

Figure 19: The effect of modification rate β on a single-dose vaccinated population.

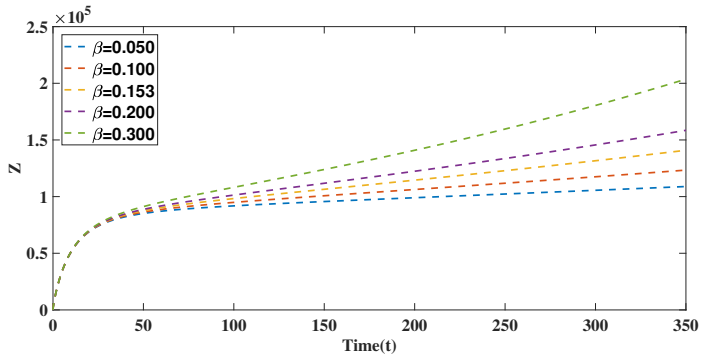

Figure 20: The effect of modification rate β on a double dose vaccinated population.

Table 1: Parameter values of the model [45].

Parameter	Value	Parameter	Value
δ	$\frac{1}{69.66\times365}$	ϕ_x	0.0105
Λ	5402.74	ϕ_y	0.0036
υ_x	0.0236	ϕ_z	0.0045
υ_y	0.0131	ω_x	$\frac{1}{15}$
υ_z	0.0121	ω_y	$\frac{1}{15}$
ς	0.1310	ω_z	$\frac{1}{15}$
α	0.3851	β	0.1536

investigations. The estimated value of the control reproduction number $\mathcal{R}_0$, for the COVID-19 outbreaks is 1.08.

According to Figure 1, $\mathcal{R}_0$ gradually lowers as α and β drop. This indicates that when infected cases are strictly diagnosed, $\mathcal{R}_0$ gradually decreases as well i.e. the rate of infection of spread gradually diminishes. Figure 2 depicts that $\mathcal{R}_0$ grows gradually as ς and α progressively rise and fall respectively. In Figure 3, ς gradually increases and β gradually decreases, $\mathcal{R}_0$ is progressively reduced.

Figure 5 and Figure 6 display the behaviors of those susceptible and those exposed over time in days, together with variations in the memory index μ at various values (0.7, 0.75, 0.8, 0.85, 0.9, 0.95, and 1). As the value of μ decreases, the number of susceptible individuals declines rapidly to zero, while the growth rate of the exposed slows correspondingly.

The action of infected individuals in Figure 7 who did not receive any vaccination $X(t)$ is illustrated, Figure 8 displays infected individuals who were given the vaccine for the first time $Y(t)$, and Figure 9 shows infected individuals who were given the second (whole) dose of the immunization $Z(t)$ along with the variation in the memory index μ at various values of 0.7, 0.75, 0.8, 0.85, 0.9, 0.95, and 1 overtime in days. For unvaccinated individuals, symptomatic cases increase rapidly with non-integer values of μ, but the infection rate declines as μ decreases. It also represents that the number of infected individuals is substantially fewer at a quicker rate ($\mu = 0.7$). In contrast, for vaccinated individuals, both after the first dose and full vaccination, the number of symptomatic cases rises with varying values of μ, reflecting the impact of vaccination on disease progression.

Furthermore, Figure 10 and Figure 11 depict the behaviors of recovered individuals, and dead individuals, against time, in days, with variations in the memory index μ, at various values of 0.7, 0.75, 0.8, 0.85, 0.9, 0.95, and 1. The graphs show that people recover more quickly as μ increases, while the number of individuals in the death category decreases with lower values of μ.

Figure 12 and Figure 13 present the behavior of individuals who did not receive any vaccination and were given the vaccine of the first dose for the time with the variation in the transmission rate ς. Figure 14 shows the impact of the transmission rate ς on a population that has received a double vaccination dose. The infection rate decreases over time across all three figures, indicating a general decline in infection rates, likely due to a combination of factors, such as population immunity, behavior changes, or other interventions. Among non-vaccinated individuals, the infection rate decreases but remains consistently higher compared to the vaccinated groups, indicating a lack of protective effects. With partial vaccination, the infection rate decreases faster than the unvaccinated group, suggesting that even a partial vaccination reduces the infection rate significantly. Full vaccination results in the steepest decline, demonstrating the highest level of protection and the cumulative efficacy of two doses.

Figures 15, 16, and 17 illustrate the effect of modification rate α on unvaccinated, single-dose, and double-dose vaccinated populations, respectively. The modification factor α which influences disease transmission or susceptibility, shows distinct trends across these groups. Among unvaccinated individuals, α decreases modestly over time but remains higher than in vaccinated groups, indicating a relatively stable yet higher risk of infection modification. In single-dose vaccinated individuals, α shows a more noticeable decline, reflecting the partial vaccine's effectiveness in reducing susceptibility or transmission rate. For double-dose vaccinated

individuals, α decreases rapidly, indicating the most substantial reduction in infection modification and demonstrating the enhanced resistance conferred by full vaccination.

Similarly, the effect of modification rate β on the unvaccinated, single-dose, and double-dose vaccinated populations are depicted in Figures 18, 19, and 20 respectively. The modification rate β shows a decreasing trend in all groups, potentially representing decreasing infection severity or progression rates. Among unvaccinated individuals, β decreases but remains relatively high, highlighting a greater likelihood of severe progression or limited protection. A decline in single-dose vaccinated people compared to the unvaccinated group indicates that a single dose significantly reduces infection severity or progression. For double-dose vaccinated individuals, β shows the most rapid and substantial decrease, suggesting that full vaccination offers the greatest protection against severe progression or susceptibility to infection modifications.

9. Conclusion

In this study, a fractional-order mathematical model with a non-local kernel has been developed to investigate the post-vaccination dynamics of COVID-19 transmission. The proposed framework incorporates vaccination effects and memory-dependent transmission dynamics, allowing a more realistic representation of population-level behavioral persistence and delayed immune responses. The existence of equilibrium points was established, and the basic reproduction number $\mathcal{R}_0$ was derived using the next-generation matrix approach, providing a clear threshold criterion for disease persistence or elimination.

Theoretical analysis confirms that the disease-free equilibrium is locally asymptotically stable when $\mathcal{R}_0 < 1$, while instability arises when $\mathcal{R}_0 > 1$. Numerical simulations were employed to illustrate the analytical findings and to explore the influence of key epidemiological parameters. In particular, the sensitivity analysis shows that transmission-related parameters and the recovery rates of unvaccinated individuals play a dominant role in shaping disease dynamics, indicating that targeted interventions targeting these groups remain crucial even in the post-vaccination phase.

The incorporation of fractional-order derivatives with a Mittag-Leffler kernel reveals that memory effects significantly influence the evolution of epidemiological compartments. Variations in the memory index alter the rate at which infections rise or decline, emphasizing the role of persistent behavioral patterns, delayed immune waning, and sustained vaccination effects. These findings underline the importance of maintaining long-term preventive measures alongside vaccination campaigns.

Overall, the proposed model provides valuable qualitative insights into COVID-19 transmission under vaccination and memory effects. The results support implementing strategies to reduce the effective reproduction number, including improving vaccine uptake, adherence to preventive measures, and timely medical intervention. Such approaches are essential for minimizing infection prevalence and disease-related burden while supporting evidence-based public health planning.

9.1. Future Scope

The present study focuses on the qualitative and theoretical analysis of vaccination-driven COVID-19 dynamics using fractional-order operators. Several meaningful extensions may be explored in future research. First, the model can be extended to include booster vaccination strategies, age-structured populations, or waning immunity to better capture long-term epidemic evolution. Second, rigorous data-driven calibration and uncertainty quantification may be incorporated to enhance predictive accuracy and policy relevance.

Further analytical developments, such as global stability analysis using Lyapunov functions, bifurcation analysis around $\mathcal{R}_0 = 1$, and detailed convergence studies of numerical schemes, also present promising directions. Additionally, the framework may be adapted to study emerging variants or applied to other infectious diseases where memory effects and delayed responses play a significant role. These extensions would further strengthen the applicability of fractional-order models in public health decision-making.

Declaration of competing interest: The authors declare that they have no known competing financial interests or personal relationships that could have appeared to influence the work reported in this paper.
Funding: This study received no specific financial support.
Data availability: No data was used for the research described in the article.

References

[1] G. Agarwal, M. Mohan Singh, D. L. Suthar, and S. D. Purohit. Analysis and estimation of the covid-19 pandemic by modified homotopy perturbation method. *Applied Mathematics in Science and Engineering*, 31(1):2279170, 2023. 1

[2] H. Agrawal, A. Singh, H. Sharma, S. Purohi, et al. Age-based investigation of covid-19 prevalence in ethiopia using mathematical modelling. *South East Asian Journal of Mathematics & Mathematical Sciences*, 20(1), 2024. 1

[3] M. Alqhtani, L. Sadek, and K. M. Saad. The mittag-leffler–caputo–fabrizio fractional derivative and its numerical approach. *Symmetry*, 17(5):800, 2025. 1

[4] A. Atangana and D. Baleanu. New fractional derivatives with nonlocal and non-singular kernel: theory and application to heat transfer model. *arXiv preprint arXiv:1602.03408*, 2016. 1, 2.3, 2.5

[5] M. Aychluh, S. D. Purohit, P. Agarwal, and D. L. Suthar. Atangana–baleanu derivative-based fractional model of covid-19 dynamics in ethiopia. *Applied Mathematics in Science and Engineering*, 30(1):635–660, 2022. 1

[6] S. Bagcchi. The world's largest covid-19 vaccination campaign. *The Lancet. Infectious Diseases*, 21(3):323, 2021. 1

[7] B. Bhatia, S. Bhatter, S. D. Purohit, D. Baleanu, and D. L. Suthar. A fractional model based on caputo derivative for tuberculosis transmission using real data from kenya. *Scientific Reports*, 2025. 6.2

[8] S. Bhatter, B. Bhatia, S. Kumawat, and S. D. Purohit. Modeling and simulation of covid-19 disease dynamics via caputo-fabrizio fractional derivative. *Computational Methods for Differential Equations*, 13(2), 2025. 1

[9] S. Bhatter, S. Kumawat, B. Bhatia, and S. D. Purohit. Analysis of covid-19 epidemic with intervention impacts by a fractional operator. *An International Journal of Optimization and Control: Theories & Applications (IJOCTA)*, 14(3):261–275, 2024. 1

[10] S. Bhatter, S. Kumawat, S. D. Purohit, and D. Suthar. Mathematical modeling of tuberculosis using caputo fractional derivative: a comparative analysis with real data. *Scientific Reports*, 15(1):12672, 2025. 7

[11] S. Boulaaras, Z. U. Rehman, F. A. Abdullah, R. Jan, M. Abdalla, and A. Jan. Coronavirus dynamics, infections and preventive interventions using fractional-calculus analysis. *Aims Math*, 8(4):8680–8701, 2023. 1

[12] K. M. Bubar, K. Reinholt, S. M. Kissler, M. Lipsitch, S. Cobey, Y. H. Grad, and D. B. Larremore. Model-informed covid-19 vaccine prioritization strategies by age and serostatus. *Science*, 371(6352):916–921, 2021. 1

[13] C. Chakraborty and G. Agoramoorthy. India's cost-effective covid-19 vaccine development initiatives. *Vaccine*, 38(50):7883, 2020. 1

[14] K. G. M. Danabal, S. S. Magesh, S. Saravanan, and V. Gopichandran. Attitude towards covid-19 vaccines and vaccine hesitancy in urban and rural communities in tamil nadu, india–a community-based survey. *BMC Health Services Research*, 21:1–10, 2021. 1

[15] K. Dietz and J. A. P. Heesterbeek. Daniel bernoulli's epidemiological model revisited. *Mathematical biosciences*, 180(1-2):1–21, 2002. 1

[16] K. D. Elgert. *Immunology: understanding the immune system*. John Wiley & Sons, 2009. 1

[17] B. H. Foy, B. Wahl, K. Mehta, A. Shet, G. I. Menon, and C. Britto. Comparing covid-19 vaccine allocation strategies in india: A mathematical modelling study. *International Journal of Infectious Diseases*, 103:431–438, 2021. 1

[18] M. Fudolig and R. Howard. The local stability of a modified multi-strain sir model for emerging viral strains. *PloS one*, 15(12):e0243408, 2020. 1

[19] H. Habenom, M. Aychluh, D. L. Suthar, Q. Al-Mdallal, and S. D. Purohit. Modeling and analysis on the transmission of covid-19 pandemic in ethiopia. *Alexandria Engineering Journal*, 61(7):5323–5342, 2022. 1

[20] Z. Hammouch, M. Yavuz, and N. Özdemir. Numerical solutions and synchronization of a variable-order fractional chaotic system. *Mathematical Modelling and Numerical Simulation with Applications*, 1(1):11–23, 2021. 1

[21] H. Jain and A. K. Sinha. Analysis of quarantine norms and their healthcare benefits for covid-19. In *International Conference on Biomedical Engineering Science and Technology*, pages 256–269. Springer, 2023. 1

[22] W. O. Kermack and A. G. McKendrick. A contribution to the mathematical theory of epidemics. *Proceedings of the Royal Society of London. Series A, Containing papers of a mathematical and physical character*, 115(772):700–721, 1927. 1

[23] S. Kumawat, S. Bhatter, B. Bhatia, S. D. Purohit, H. M. Baskonus, and D. L. Suthar. Novel application of q-hagtm to analyse hilfer fractional differential equations in diabetic dynamics. *Mathematics and Computers in Simulation*, 2025. 1

[24] S. Kumawat, S. Bhatter, D. Suthar, S. Purohit, and K. Jangid. Numerical modeling on age-based study of coronavirus transmission. *Applied Mathematics in Science and Engineering*, 30(1):609–634, 2022. 4.2

[25] Z. Liu, P. Magal, O. Seydi, and G. Webb. Predicting the cumulative number of cases for the covid-19 epidemic in china from early data. *arXiv preprint arXiv:2002.12298*, 2020. 1

[26] K. Logeswari, C. Ravichandran, and K. S. Nisar. Mathematical model for spreading of covid-19 virus with the mittag–leffler kernel. *Numerical Methods for Partial Differential Equations*, 40(1):e22652, 2024. 1

[27] N. Madani, Z. Hammouch, and E.-H. Azroul. New model of hiv/aids dynamics based on caputo–fabrizio derivative order: Optimal strategies to control the spread. *Journal of Computational Science*, page 102612, 2025. 1

[28] M. Makhoul, H. H. Ayoub, H. Chemaitelly, S. Seedat, G. R. Mumtaz, S. Al-Omari, and L. J. Abu-Raddad. Epidemiological impact of sars-cov-2 vaccination: mathematical modeling analyses. *Vaccines*, 8(4):668, 2020. 1

[29] M. Manivel and A. Venkatesh. Numerical simulations and analysis of monkeypox disease under fractional order mathematical models. *Advances in Mathematical Sciences and Applications*, 34(2):679–701, 2025. 1

[30] M. Manivel, A. Venkatesh, K. A. Kumar, M. P. Raj, S. E. Fadugba, and M. Kekana. Quantitative modeling of mon-

keypox viral transmission using caputo fractional variational iteration method. *Partial Differential Equations in Applied Mathematics*, 13:101026, 2025. 5.2

[31] M. Meena, M. Purohit, Shyamsunder, S. D. Purohit, and K. S. Nisar. A novel investigation of the hepatitis b virus using a fractional operator with a non-local kernel. *Partial Differential Equations in Applied Mathematics*, 8:100577, 2023. 1

[32] F. Nabizadeh, E. Ramezannezhad, K. Kazemzadeh, E. Khalili, E. M. Ghaffary, and O. Mirmosayyeb. Multiple sclerosis relapse after covid-19 vaccination: A case report-based systematic review. *Journal of Clinical Neuroscience*, 104:118–125, 2022. 1

[33] N. Namdev and A. K. Sinha. Prediction of the supportive vaccine type of the covid-19 for public health. *J. Math. Comput. Sci.*, 11(5):5703–5719, 2021. 1

[34] Our World in Data. Data on covid-19 (coronavirus). `https://github.com/owid/covid-19-data/tree/master/public/data`, 2022. Accessed: June 10, 2022. 8

[35] K. M. Owolabi and E. Pindza. A nonlinear epidemic model for tuberculosis with caputo operator and fixed point theory. *Healthcare Analytics*, 2:100111, 2022. 5.2

[36] R. M. Pandey, A. Chandola, and R. Agarwal. Mathematical model and interpretation of crowding effects on sars-cov-2 using atangana-baleanu fractional operator. In *Methods of Mathematical Modeling*, pages 41–58. Elsevier, 2022. 1

[37] C. A. Pearson, F. Bozzani, S. R. Procter, N. G. Davies, M. Huda, H. Jensen, M. Keogh-Brown, M. Khalid, S. Sweeney, S. Torres-Rueda, et al. Health impact and cost-effectiveness of covid-19 vaccination in sindh province pakistan. *medRxiv*, 2021. 1

[38] I. Podlubny. *Fractional differential equations: an introduction to fractional derivatives, fractional differential equations, to methods of their solution and some of their applications*. elsevier, 1998. 2.1

[39] M. P. Raj, A. Venkatesh, K. A. Kumar, and M. Manivel. Dengue transmission model in an age-structured population using delay differential equations. *Discover Public Health*, 22(1):1–20, 2025. 1

[40] R. Rappuoli, C. W. Mandl, S. Black, and E. De Gregorio. Vaccines for the twenty-first-century society. *Nature reviews immunology*, 11(12):865–872, 2011. 1

[41] L. Sadek and A. Akgül. New properties for conformable fractional derivative and applications. *Progr. Fract. Differ. Appl*, 10(3):335–344, 2024. 1

[42] L. Sadek, A. S. Bataineh, E. M. Sadek, and I. Hashim. A general definition of the fractal derivative: Theory and applications. *AIMS Mathematics*, 10(7):15390–15409, 2025. 1

[43] L. Sadek, T. A. Lazar, and I. Hashim. Conformable finite element method for conformable fractional partial differential equations. *AIMS Math*, 8(12):28858–28877, 2023. 1

[44] A. Shaikh, I. Shaikh, and K. Nisar. A mathematical model of covid-19 using fractional derivative: Outbreak in india with dynamics of transmission and control, adv. difference equations 2020 (1)(2020) 1–19. *S. Ullah et al*, 2020. 1, 5.1

[45] Shyamsunder, S. Bhatter, K. Jangid, A. Abidemi, K. M. Owolabi, and S. D. Purohit. A new fractional mathematical model to study the impact of vaccination on covid-19 outbreaks. *Decision Analytics Journal*, 6:100156, 2023. 2.2, 1

[46] A. K. Sinha and K. Soni. Fractional-order modeling of hepatitis b dynamics incorporating socio-environmental factors. *Discover Public Health*, 22(1):537, 2025. 1

[47] I. N. Sneddon. *Fourier transforms*. Courier Corporation, 1995. 2.4, 2.4

[48] K. Soni and A. K. Sinha. Modeling marburg virus control with limited hospital beds: a fractional approach. *Physica Scripta*, 100(1):015251, 2024. 6.3

[49] K. Soni and A. K. Sinha. Dynamics of epidemic model with conformable fractional derivative. *Nonlinear Science*, page 100040, 2025. 6.2

[50] K. Soni and A. K. Sinha. A novel fractional-order mathematical model for hepatitis b: impact of awareness. *International Journal of Modelling and Simulation*, pages 1–18, 2025. 1

[51] O. Thomas, J. Amos, G. O. Acheneje, E. Abah, A. B. Celestine, B. Bolaji, et al. Numerical simulation and fractional-order analysis of covid-19–zika co-infection: Impacts of vaccination, treatment, and vector control. *Nonlinear Studies*, 32(4):1465–1499, 2025. 1

[52] M. Toufik and A. Atangana. New numerical approximation of fractional derivative with non-local and non-singular kernel: application to chaotic models. *The European Physical Journal Plus*, 132:1–16, 2017. 7

[53] N. H. Tuan, H. Mohammadi, and S. Rezapour. A mathematical model for covid-19 transmission by using the caputo fractional derivative. *Chaos, Solitons & Fractals*, 140:110107, 2020. 1

[54] P. Van den Driessche and J. Watmough. Reproduction numbers and sub-threshold endemic equilibria for compartmental models of disease transmission. *Mathematical biosciences*, 180(1-2):29–48, 2002. 6.1

[55] J. Xie, X. Yan, M. A. Ali, and Z. Hammouch. A linear decoupled physical-property-preserving difference method for fractional-order generalized zakharov system. *Journal of Computational and Applied Mathematics*, 426:115044, 2023. 1

[56] A. Zeb, A. Atangana, Z. A. Khan, and S. Djillali. A robust study of a piecewise fractional order covid-19 mathematical model. *Alexandria Engineering Journal*, 61(7):5649–5665, 2022. 1